Smart Materials in Manufacturing 1 (2023) 100013

Contents lists available at ScienceDirect

Smart Materials in Manufacturing

journal homepage: www.keaipublishing.com/en/journals/smart-materials-in-manufacturing

Self-assembly meets additive manufacturing: Bridging the gap between nanoscale arrangement of matter and macroscale fabrication

Antonella Sola *, Adrian Trinchi, Anita J. Hill

Commonwealth Scientific and Industrial Research Organisation (CSIRO), Advanced Materials and Processing Program, Manufacturing Business Unit, Clayton, VIC 3168, Australia

ARTICLE INFO

Keywords:
Self-assembly
Directed assembly
Additive manufacturing
Field-assisted additive manufacturing
Nanoparticle
Patterning

ABSTRACT

New methods are emerging to combine the self-assembly of matter and additive manufacturing, so that new devices and constructs can simultaneously harness the unique molecular and nanostructural features afforded by self-assembly and the macroscale design freedom of additive manufacturing. The aim of this review is to analyse the body of literature and explore the crossover area where boundaries dissolve and self-assembly meets additive manufacturing (SAMAM). As a preliminary framework for this new area of research, the different experimental approaches to SAMAM can be grouped in three main categories, whereby SAMAM can be based on local interactions between molecules or nanoparticles, on 3D-printing induced forces, or on externally applied force fields. SAMAM offers numerous opportunities, such as the design of new printable materials, the ability to surpass conventional trade-offs in materials properties, the control of structural features across different length scales, process intensification and improved eco-sustainability. However, most research so far has been focused on polymer-based materials, and additional effort is needed to understand how SAMAM can be leveraged in metal- and ceramic-based additive manufacturing. On account of the weak inter-layer bonding often reported along the growth direction, it would also be interesting to explore whether SAMAM could effectively remediate undesidered anisotropic effects in additively manufactured parts.

1. Introduction

The advancement of precision additive manufacturing (AM, a.k.a. 3D printing), for example in nanoelectronics, optics, energy storage and harvesting, micromechanical sensing, and medicine, has the potential to benefit many areas of industry and research. Nanostructuring is key for decoupling density and structural properties, and is the steppingstone for producing new materials, such as ultra-lightweight constructs and damage-tolerant materials [1]. Due to the increasing industrial relevance of additive nano-manufacturing, 3D printers that work at the nanoscale are being explored. For example, light-based 3D printing technologies such as two-photon polymerisation [2] and micro-stereolithography [3] polymerise photocurable resins with sub-microscale or even nanoscale resolution (for the sake of clarity, a brief description of the AM techniques mentioned in the text and their acronyms are provided in Table 1). This precision allows devices and hierarchical structures to be fabricated with features ranging from the nanoscale to the microscale [4]. However, in spite of their tremendous potential to revolutionise the field of nano- and micro-AM, these new technologies are still a rarity in industrial settings, and their transferability "from lab to fab" is uncertain [5,6]. On the other hand, quite often present-day approaches to manipulating the properties of AM parts at the nanoscale rely on the progressive reduction in size of existing printing hardware. Although these top-down methods may appear to be intuitive and straightforward as they build up on well-established printing mechanisms, they are severely impeded in controlling the material's nanostructure as a consequence of the technological limits to miniaturisation [7]. Conversely, the bottom-up approach encourages creation of hierarchical order as a result of the

* Corresponding author.
E-mail address: antonella.sola@csiro.au (A. Sola).

Production and Hosting by Elsevier on behalf of KeAi

https://doi.org/10.1016/j.smmf.2022.100013
Received 26 October 2022; Received in revised form 25 November 2022; Accepted 26 November 2022
Available online 08 December 2022

Table 1
Functioning mechanism of AM technologies mentioned in the main text (listed in alphabetical order).

AM Technique	ISO/ASTM 52900 category	Functioning mechanism
Bioprinting	Various	Any AM technology that allows living cells, growth factors, and extra-cellular matrix (ECM) components to be incorporated in the printing material.
Directed energy deposition (DED)	Directed energy deposition (DED)	The feedstock, typically a metal or alloy in powder or wire form, is fed into the melt pool which is being generated on the surface of the part by a laser or electron beam.
Digital light processing (DLP)	Vat photopolymerisation (VPP)	DLP, like stereolithography (SLA), builds up 3D objects through the selective curing of a photosensitive resin. In DLP, a digital projector flashes the image of the whole layer across the resin vat at once.
Direct ink writing (DIW)	Material extrusion (MEX)	DIW is mainly applied in meso- and micro-scale manufacturing. The liquid-phase ink is extruded through a thin nozzle moving according to a computer-controlled toolpath. Parts can be printed layer-by-layer. Otherwise, continuous 3D traces can be dispensed in a supporting bath. This may require photocuring to stabilise the geometry.
(Direct) inkjet printing	Material jetting (MJT)	(Direct) inkjet printing is conceptually similar to conventional inkjet printing on paper, in that a printhead ejects fine droplets of material on the substrate to draw the desired layer geometry, then the process is repeated layer-by-layer. Droplets can be ejected on demand or continuously. Inks are often low-viscosity resins (polymer solutions, molten polymers, photocurable thermosets) or composites.
Drop on demand (DOD)	Material jetting (MJT)	DOD is a variant of inkjet printing in which fine droplets of material are ejected where needed. The deposition is thus discontinuous.
Electron beam melting (EBM)	Powder bed fusion (PBF)	EBM uses an electron beam to locally fuse a thin layer of powder, which must be an electrically conductive material, typically a metal or alloy. The electron beam draws the desired geometry, then a rack distributes a new layer of fresh powder on top of the previous one, and the process is repeated until completion of the 3D part. In principle, the technique is similar to selective laser sintering (SLS) and selective laser melting (SLM).
Fused filament fabrication (FFF)	Material extrusion (MEX)	FFF (a.k.a. fused deposition modeling, FDM) uses a thermoplastic or composite filament as feedstock. The filament is pushed in the liquefier, heated, melted and extruded on the substrate (or previous layers). For each layer, the printhead moves in X and Y directions to draw the desired geometry.
Micro-stereolithography (micro-SLA or μ-SLA)	Vat photopolymerisation (VPP)	Micro-SLA is a form of high-resolution stereolithography achieved through process improvement.
Selective laser melting (SLM)	Powder bed fusion (PBF)	SLM uses a laser to locally melt a thin layer of powder, quite often made of a metal, alloy or composite. The laser draws the desired geometry, then a rack distributes a new layer of fresh powder on top of the previous one, and the process is repeated until completion of the 3D part. In principle, the technique is similar to SLS and EBM.
Selective laser sintering (SLS)	Powder bed fusion (PBF)	SLS uses a laser to locally sinter a thin layer of powder, quite often made of a thermoplastic or composite material. The laser draws the desired geometry, then a rack distributes a new layer of fresh powder on top of the previous one, and the process is repeated until completion of the 3D part. In principle, the technique is similar to SLM and EBM.
Stereolithography (SLA)	Vat photopolymerisation (VPP)	SLA is based on the laser-induced polymerisation of a photosensitive resin. The laser scans the desired geometry to complete one layer, then the process is repeated layer-by-layer.
Two-photon polymerisation (2PP)	Vat photopolymerisation (VPP)	2PP (a.k.a. direct laser writing, DLW) consists in the ultra-high resolution photocuring, voxel-by-voxel, of a photosensitive resin induced by two photon absorption.

spontaneous assembly of matter, thus breaking the dependency on printing equipment. This is where self-assembly meets additive manufacturing (SAMAM).

Whilst many definitions have been formulated for “self-assembly”, the term is employed here according to the intuitive understanding of the autonomous positioning of pre-existing components (“building blocks” - for example, living cells in biology, as well as atoms, molecules, and particles of varying size in chemistry and engineering). This usually happens through the creation of a bond (quite often, a reversible bond) between the building blocks once they have moved to the desired mutual position, and ultimately leads to the appearance of order from disorder [8,9]. According to this definition, “self-assembly” in SAMAM verges on the mere spatial arrangement of the constituents - atoms, molecules, (nano)particles - used for printing. This version of self-assembly is also consistent with the definition given by Wintzheimer et al. [10], whereby self-assembly is the ordering of “individual components into organized structures solely through interactions among the components that minimize the free energy”. Conversely, self-assembly in biological systems is inseparably coupled with the genesis of matter. According to the description proposed by Nguyen et al. [11], cells can be regarded as nanomaterial factories, since cells are able to source basic molecules from the environment and to refashion them into new complex biological materials that match precise context-dependent functional requirements. In living organisms, compatibly with ageing and major accidents, cells are also able to repair and maintain these tissues over time. The recent advancement of synthetic biology has led to the successful development of engineered living materials (ELMs), which are biohybrid constructs composed of living cells that form or assemble the material itself, or modulate its functional performance [11]. A practical example is offered by self-healing biological concrete, which contains the spores of special bacteria that are able to “eat” (enzymatically digest) small amounts of nutrients embedded in the concrete and secrete calcium carbonate. If the concrete matrix is damaged, water can penetrate through the micro-cracks and prompt the spores to germinate. The bacteria are then able to multiply and precipitate minerals, especially calcium carbonate, that heal the cracks [12]. Engineered living materials are theoretically compatible with 3D printing, for example through the bioprinting of living cells embedded in hydrogels [13]. However, the spectrum of materials that can be biologically engineered through living cells is still very limited. This justifies the initial assumption of SAMAM as working with spontaneous patterning, as opposed to biological creation of new materials and tissues.

Although the integration of self-assembly and AM is still an emerging field of research, the body of literature is flourishing, with an exponential growth starting from 2018. The impetus for SAMAM may have originated from a combination of factors. On the one hand, the Covid-induced sanitary emergency has called for leaner fabrication technologies and for more secure supply chains [14]. In this regard, AM has proved to be a secure method for producing goods and granting services through distributed manufacturing, thus largely contributing to sovereign capability [15–17]. On the other hand, many AM technologies have reached their technological maturity, but are currently striving for extended functionality through new printable materials [18–21]. For example, it has been estimated that the number of materials suitable for selective laser melting (SLM), which is the most popular metal AM method, sits at around 50 [22]. If only market-ready materials are considered, this number narrows down to around 10-12, with stainless steel (e.g., 316L), tool steel (e.g., 17-4 PH), AlSi10Mg, TiAl6V4, CoCr and Inconel 718 being the most relevant ones [23] This is in stark contrast to the palette of metals and alloys routinely processed in conventional manufacturing, which counts more than 5500 options [24].

Whilst describing numerous practical examples of SAMAM, the main

goal of this review article is to analyse, discuss and, wherever possible, classify the different strategies that can be deployed in order to conjugate self-assembly and AM. The state of the art of SAMAM is critically investigated in order to capture proven results, existing challenges and emerging opportunities. In the burgeoning field of SAMAM, a clarifying roadmap is still missing, and urgently needed. Such a roadmap to SAMAM can inform researchers and developers of the potentiality of this disruptive technology and drive its future growth.

2. Self-assembly and 2/3/4D printing

As presented in the following paragraphs, a survey of the literature reveals two major trends that integrate printing technologies and self-assembly (or directed assembly, as explained below), which consist of (i) printing of 2D self-assembled patterns (examined in Section 2.1), and (ii) AM of 3D parts combined with self-assembly of matter (Section 2.2). Recent studies have also demonstrated the feasibility of (iii) merging self-assembly with 4D printing (defined in Section 2.3) as an advancement of self-assembly-assisted 3D printing.

2.1. Printing of self-assembled 2D patterns

As recently reviewed by Zhao et al. [25], there is increasing interest in producing controlled nanoparticle (NP) patterns through 2D printing. Largely tapping into the existing knowledge in lithography and contact printing, NPs are arranged according to a bespoke 2D design using templates, stamps and screens. Otherwise, direct ink writing (DIW) through miniaturised nozzles enables the selective deposition of NPs on a substrate. Dip-pen assembly is an alternative approach to direct writing, wherein the nozzle is substituted by the tip of an atomic force microscope. The tip is preliminary dip-coated with the NP ink and then moved to draw the desired pattern according to a computer-controlled toolpath.

Attempts have also been made to scale these technologies up to obtain 3D objects by repeating the deposition layer-upon-layer. For example, Park et al. [26] built a surface-enhanced Raman spectroscopy (SERS) substrate by multi-step micro-contact (transfer) printing. The master mould used for transfer printing was obtained through the combination of photolithography and directed self-assembly of block copolymers (BCPs) according to a protocol previously outlined by Yim et al. [27]. Although geometric features could be closely controlled at the nanoscale, only few nanosheets (specifically, two or four layers [26]) could be applied, and the lateral size of the printed device was also in the sub-micrometre range. Otherwise, nozzle-based 2D printing by DIW can be leveraged to deposit NP inks onto selected areas of a 3D substrate. This was the target of the research conducted by Siebert et al. [28], who developed an acetone sensor based on the DIW of iron and copper microparticles dispersed in an ethanol solution of polyvinylbutyral (PVB). The ink was extruded on glass slides to produce meandering printed stripes. After printing, the growth of nanorods and nanospikes required for bridging the iron and copper particles was induced by thermal annealing, followed by gold sputtering. In principle, the sensor could be peeled off from the glass substrate before receiving the thermal annealing, and then transferred onto a curved geometry. However, in spite of the capability of producing fully 3D parts by DIW (as further discussed in the following sections), the protocol developed by Siebert et al. [28] appears to be still confined to obtaining decorated surfaces.

These printing techniques are poised to produce 2D constructs with a close control on nanoscale features. However, they are not primarily intended to complete 3D objects and, for this reason, they are not discussed in detail in this paper, whose aim is instead to explore the utility of self-assembly in AM. This is consistent with the definition of AM as being a group of "technologies that successively join material to create physical objects as specified by 3D model data". In other words, AM "applies the additive shaping principle and thereby builds physical three-dimensional (3D) geometries by successive addition of material … usually layer upon layer" [29]. Ultimately, SAMAM is thus meant to be the conjugation of self-assembly with AM, including 3D and 4D printing.

2.2. AM of 3D parts combined with self-assembly

Early research in bottom-up AM of structured materials was based on chemical vapour deposition (CVD) and physical vapour deposition (PVD) [30]. Back in 2003, for example, Li et al. [31] demonstrated a bottom-up approach for producing multilevel interconnects based on CVD. Ordered arrays of self-standing carbon nanotubes (CNTs) were grown by plasma-enhanced CVD, embedded in SiO_2 (as the dielectric gap filling) by CVD using tetraethylorthosilicate (TEOS), and planarised by chemical mechanical polishing (CMP). However, CVD and PVD are better suited to producing a thin film deposit on a pre-existing substrate, rather than a self-standing 3D object. Although the exact processing conditions are material-dependent, CVD and PVD typically require high temperatures and high levels of purity, which may be unfeasible with some types of substrates and materials. Moreover, the significant power consumption and the extremely long deposition times make these techniques uneconomical [30,32].

Nowadays, the self-assembly of matter in fully 3D parts is harnessed through three main mechanisms, including (i) the development of new printable materials and constructs that spontaneously self-arrange through intermolecular and surface forces, (ii) the spatial ordering of matter dictated by the forces that are spontaneously generated upon printing, and (iii) the re-distribution or re-orientation of fillers under the action of external forces or fields (further detail in Section 3).

In principle, self-assembly should occur naturally under thermodynamic driving forces, because the system evolves towards its lowest energy state. However, some systems may require an input of energy or external forces to evolve and produce a particular structure or assembly [4,33,34]. Accordingly, "self-assembly" and "directed assembly" (a.k.a. "engineered assembly" or "self-organisation") should be kept separate as two different phenomena, since the former is the aggregation of components through local interactions close to equilibrium, whereas the latter is the achievement of desired patterns of molecules or particles driven by external fields or forces and usually occurring out of equilibrium. Considering this distinction, both the action of inherent forces caused by the printing process and the implementation of external forces or fields (corresponding to mechanisms (ii) and (iii) above) should be labelled as "directed assembly", rather than "self-assembly" (which would lead to the alternative acronym "directed assembly meets additive manufacturing", DAMAM). Nonetheless, as schematised in Fig. 1, the following sections account for all of them under the common umbrella of SAMAM, as they all represent practical means of targeting the nanostructure in AM through the properties of matter, as opposed to the miniaturisation of the printing equipment.

In spite of the increasing success of AM for the production of personalised food, the present review only considers structural and functional materials, but not edible ones, which are designed to meet different targets such as new textures and increased nutritional value [35]. Readers interested in SAMAM of food may find examples and a list of updated references in the contributions by H. Wang et al. [36,37] and by Pulatsu et al. [38].

2.3. Self-assembly and 4D printing

Inspired by nature, 4D printing is the new frontier in AM, as it is the combination of 3D printing with time as the fourth dimension to produce stimuli-responsive parts that change their shape or properties in response to a specific environmental trigger, such as a variation in temperature, applied load, light, or pH/acidity [39–44]. 4D printed parts can thus be regarded as "animate structures", as they are able to sense changes in their environment and respond accordingly (i.e., they are "adaptive"). In doing so, they can change their attributes (i.e., they are "active") without being externally controlled (i.e., they are "autonomous") [45].

As exemplified by relevant examples in the following sections,

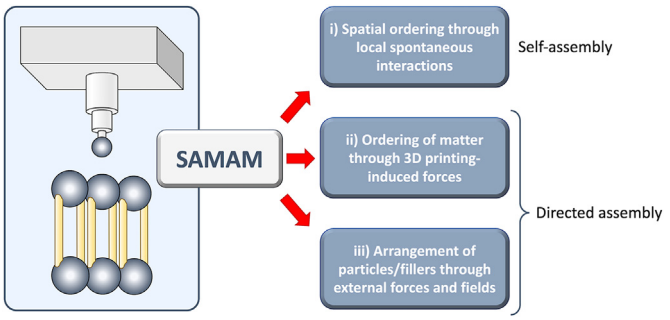

Fig. 1. SAMAM: Different approaches to combining additive manufacturing and self-assembly or directed assembly of matter.

SAMAM can contribute to the advancement of 4D printing, since hierarchical architectural modification based on self-assembly can be leveraged for programming new adaptive materials that deploy a controlled morphing ability.

3. SAMAM: A bottom-up approach to 3D and 4D printing

Whilst several approaches to SAMAM have already been experimented in the literature, they can be generally classified as (i) SAMAM through local interactions between molecules or NPs, (ii) SAMAM through forces that spontaneously act upon printing, and (iii) SAMAM through externally applied force fields. While the following sections provide additional information and numerous examples for each SAMAM method, Fig. 2 demonstrates some examples as a form of introduction.

3.1. SAMAM through local interactions

Hierarchical order in AM constructs can be based on the spontaneous arrangement of individual building blocks, which can be either molecules or NPs, through skilfully governed attraction/repulsion forces.

3.1.1. Molecular self-assembly

Direct AM through self-assembly of individual molecules was demonstrated by Hamoudi et al. [46]. The obtained 3D structures were hierarchical assemblies whereby dithiol molecules self-assembled into monolayers at liquid-liquid interfaces, whilst subsequent monolayers were added on top of each other with metal ions working as mediators for inter-layer bonding. The layer-wise addition of self-assembled monolayers (SAMs) led to the build-up of defect-free materials with outstanding self-healing properties. However, the liquids containing the dithiol molecules could only be injected with a flow speed of 650 $\mu L\ m^{-1}$ and the vertical nozzle speed was adjusted to around 0.2 $mm\ s^{-1}$ in order to match the growth rate of the self-assembled structure. As such, the translation of these periodic stacks of metal-based self-assembled monolayers to fabricate macroscale devices may still be challenging.

Self-assembly of polymer molecules is a very popular method to obtain new printable materials, especially for material extrusion AM ("MEX") techniques. According to the IUPAC definition, a supramolecule is "a system of two or more molecular entities held together and organized by means of intermolecular (noncovalent) binding interactions" [47]. Intuitively, if the hierarchical structure of matter could be translated into the mathematical language of proportions, supramolecules would be to molecules as molecules are to atoms according to the (theoretical) equation:

$$\text{supramolecules:molecules} = \text{molecules:atoms} \quad (1)$$

In other terms, atoms are the building blocks of molecules, much as molecules are the building blocks of supramolecules, even if the nature and strength of the chemical bonds and interactions are likely different within individual molecules and supramolecules.

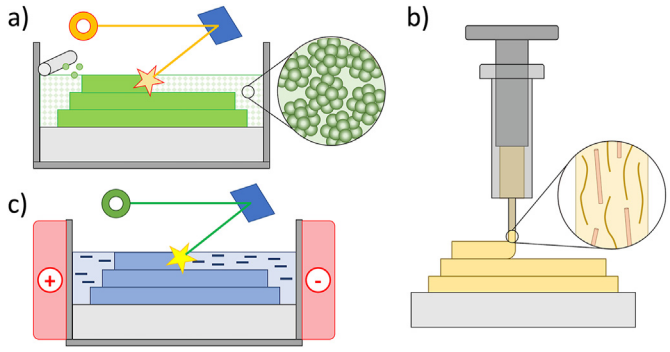

Fig. 2. Different experimental approaches to SAMAM. (a) As an example of SAMAM through local interactions in selective laser sintering (SLS), conventional feedstocks can be replaced by supraparticles, whereby each particle is actually the result of the self-assembly of primary nanoparticles through spray drying. (b) As an example of 3D printing-enabled SAMAM in materials extrusion (MEX), the flow through the print nozzle unavoidably produces shear stresses that preferentially align the molecular chains of the polymer matrix as well as the elongated fillers, if present. (c) As an example of field-assisted SAMAM in vat photopolymerisation (VPP), elongated fillers can be preferentially oriented under the action of an electric field applied to the resin vat.

Citing Jean-Marie Lehn, supramolecular chemistry is thus "a chemistry beyond the molecule", as it is "the buildup (synthesis!) of discrete or extended assemblies of chemical objects" [48–50]. Supramolecular polymers are able to self-assemble through non-covalent interactions, such as supramolecular hydrogen bonding, $\pi - \pi$ stacking, metal complexation, and ionic interactions. Since these bonds are dynamic and reversible, supramolecular polymers feature superior characteristics over conventional polymers, such as enhanced material strength and toughness, self-healing, and stimuli responsiveness. As recently discussed by Rupp and Binder [51], supramolecular polymers offer additional advantages in the realm of AM, as the inter-molecular interactions can be chemically programmed to meet the demanding rheological requisites for successful printing by different techniques, including MEX, vat photopolymerisation (VPP), direct inkjet printing, and bioprinting. Moreover, supramolecular interactions like hydrogen bonds work as non-covalent crosslinkers mitigating the inter-layer adhesion issues, which are one of the main limitations to the structural integrity of AM parts along the growth direction.

Andriamiseza et al. [52], for example, recently demonstrated the effectiveness of self-assembled low molecular weight hydrogels for the AM of scaffolds for cell culture by DIW. Low molecular weight gelators self-assemble into fibre- or flake-like structures or other anisotropic aggregates thanks to directional non-covalent interactions. The force of these interactions can be governed through the molecular structure in order to produce more or less dynamic assemblies. Meanwhile, the absence of covalent bonds makes these "molecular gels" very delicate, but also very soft, and thus ideal for receiving vulnerable and flexible cells like neurons. The range of application for molecular gels can be increased by mixing different gelators, for example peptide- and carbohydrate-based gelators. Different gelation mechanisms can also be pursued. Multi-material DIW of low molecular weight hydrogels having different solubility in water enables the fabrication of imbricated structures, wherein a sacrificial ink is printed as a temporary framework to support the part's geometry until complete consolidation of the persistent ink occurs [52].

Whilst the research by Andriamiseza et al. [52] harnessed supramolecular self-assembly through cohesive non-covalent forces, Bai et al. [53] were the first to observe that a ketone homopolymer is able to self-assemble into nano- and micro-gels through covalent crosslinking, which represents an instance of covalent supramolecular arrangement. The size of the hydrogels from below 10 nm to above 100 nm can be finely tuned through the covalent crosslinking rate. Microgels, in their

turn, self-organise into granular fibres that are suitable for direct 3D printing of porous scaffolds. Although the printed geometries are relatively simple, the self-assembled fibrous structures may be useful in drug delivery and tissue engineering.

Honaryar et al. [54] were able to fabricate soft constructs by means of the spontaneous separation of amphiphilic materials (such as lipids or surfactants) at the interface between immiscible liquids. To this aim, a low-viscosity aqueous solution of a proper surfactant was injected into a polar oil phase to build up the desired soft object (which is an example of MEX through liquid-in-liquid printing). The molecules of the surfactant preferentially migrated to the interface between aqueous solution and oil medium, where they self-assembled in ordered nanostructures, either hexagonal or lamellar, and stabilised the printed object. However, since this scaffolding effect was just temporary, the water-based solution also contained a prepolymer and an initiator that were photocured under UV light during and immediately after printing, in order to fix the geometry permanently.

The complicated interplay of attractive and repulsive forces acting between miscible and immiscible compounds also underpins the functioning mechanism of BCPs, which can be mixed with resins to improve the mechanical properties, especially the toughness, of parts produced by VPP. BCPs consist of two (or more) polymer blocks that have different chemical features in spite of being covalently bonded to each other. In more detail, one block is usually miscible, and hence compatible with the resin, while the other block is immiscible. BCPs naturally tend to segregate in order to minimise the energetically unfavourable interactions between dissimilar blocks. However, due to the covalent bond, the blocks cannot separate macroscopically, and phase separation can only occur at a length scale comparable to the size of the individual blocks. Depending on the chemistry and the relative amounts of resin and BCPs, different configurations are possible, ranging from individual roundish BCP particles to larger aggregates, to worm-like structures. Regardless of the morphology, achieving a complete microphase separation is crucial, because otherwise the excess BCPs would disperse into the resin and work as plasticiser, thus decreasing the stiffness of the resin. In principle, the self-assembly of BCPs in a photocurable resin may occur prior to or while curing. However, according to the results reported by Demleitner et al. [55], completing the network formation before curing would be preferable in order to minimise the harmful condition of partial microphase separation. In this way, the presence of the BCP domains produces an effective toughening mechanism via cavitation and shear yielding.

In synthesis solutions, if the concentration is high enough and exceeds the “critical micelle concentration”, BCPs self-assemble and form micelles that may act as template for nanopores in hierarchical scaffolds [56]. Z. Wang et al. [57] modified the functionality of F127, a triblock copolymer composed of a central hydrophobic chain of poly(propylene oxide) flanked by two hydrophilic chains of poly(ethylene oxide), by the acryloyl substitution of the terminal hydroxyl groups. Following to the acryloyl modification, F127 molecules became photocurable, while preserving their ability to self-assemble. A printable ink was then produced by mixing the acryloylated F127 in ethanol with a bioactive glass sol, with the minor addition (0.5%) of photo-initiator. Macroporous lattice structures were 3D printed by MEX and locked in place by UV irradiation. After drying off the liquid medium, the green parts were sintered at 600 °C to obtain the final bioactive glass scaffolds. The structural characterisation revealed a multi-scale porosity that combined the extremely regular columnar nanopores (average diameter below 7 nm) originating from the F127 micellar template with the sub-millimetre grid fabricated by 3D printing. In spite of the substantial shrinkage of around 33%, the nanoscale-templated tubular pores were not destroyed, nor clogged after sintering, and the minimal presence of cracks led to a substantive compressive strength of around 2.5 MPa, thus matching the properties of trabecular bone.

BCPs can also be leveraged in DIW, as demonstrated by Bowen et al. [58]. In this research, the ink was a mixture of a preceramic polymer (polycarbosilane, PCS), with a triblock copolymer composed of poly(methyl methacrylate) (PMMA) and poly(n-butyl acrylate) (PnBA) dispersed in 1-butanol. Since the polycarbosilane and the organic solvent selectively swell the hydrophobic PnBA segments, the block copolymers segregated and self-assembled in worm-like micelles. After printing the desired lattice geometries by DIW, the nanostructure was locked in place via click chemistry (UV curing). Then, the preceramic polymer was crosslinked, and finally the polymer compounds were removed via pyrolysis at 800 °C. The obtained ceramic scaffolds featured a hierarchical porosity, wherein the microscale pores (lateral size around 400 μm) were controlled by the AM process, whilst the nanoscale pores were imposed through self-assembly of matter. Interestingly, the lattices were pliable and foldable after DIW and curing, and the received shape could be retained during pyrolysis.

3.1.2. Self-assembly of nanoparticles

Due to their small size and enormous specific surface area, NPs feature extraordinary properties [4,33]. However, translating the properties theoretically predicted of nanomaterials into functioning macroscale objects and devices may be impractical due to nonuniform dispersion and lack of alignment [32]. Currently, NPs can be easily assembled into colloidal structures that are governed by short-range intermolecular and surface forces. However, this bottom-up approach mainly results in 1D or 2D structures, whilst large-scale 3D structures are still difficult to reach [59].

In order to overcome this challenge, Tan et al. [60] defined the combination of colloidal self-assembly and DIW as “direct-write colloidal assembly”. This new approach was introduced to simultaneously enable the local control of NP organisation through evaporative colloidal self-assembly, and the global control of the part's geometry through DIW. To this aim, a colloidal suspension is fed in a custom-made DIW apparatus. A small amount of suspension is first dispensed to form a liquid bridge between the print nozzle and the substrate. This liquid bridge provides lateral confinement for the NPs to gradually accumulate on the substrate. As a solid layer appears at the base of the liquid bridge, the substrate is moved downwards at a rate matching the growth rate of the solid structure. The evaporation of the liquid carrier brings the NPs in intimate contact, which favours the establishment of inter-particle van der Waals forces that are responsible for the growth of well-ordered polycrystalline regions and, ultimately, for the stability of the part's geometry.

Tan et al. [60] demonstrated the feasibility of direct-write colloidal assembly with aqueous suspensions of monodispersed polystyrene (PS) NPs with radius ranging from 44 nm to 500 nm. Columnar structures (“towers”) were built at a speed of about 1–5 μm s^{-1}. The height varied between 1 mm and 10 mm, with an aspect ratio as high as 10. Whilst the diameter of the colloidal towers was mainly governed by the size of the print nozzle, it was possible to produce local variations resulting in hourglass-like structures through the calibrated change of the dispense rate relative to the vertical rate of motion. Helical towers were also achieved by implementing a rotating substrate. Interestingly, towers made from particles of different radius displayed structural coloration at different wavelength in the visible spectrum due to Bragg reflection. In order to provide further evidence of the versatility of direct-write colloidal assembly, towers were also built with other building blocks, such as silica NPs and gold nanocrystals.

Colloidal nanoinks are also compatible with inkjet printing, in which the ink is deposited drop-wise. Kullmann et al. [61] were able to grow micro-wires with an aspect ratio exceeding 50 by the piezoelectric drop-on-demand (DOD) deposition of a colloidal suspension of gold NPs (diameter in the 2–4 nm range) in toluene. It was observed that relatively thick wires were built up at room temperature, with an average diameter corresponding to around 5 times the diameter of the ejected drops. However, due to the enhanced evaporation of toluene, the wires became sensibly thinner, with an average diameter corresponding to around 2 times the diameter of the ejected drops, when the temperature of the substrate was raised to 60 °C. Increasing the substrate temperature also

sped up the growth rate of the micro-wires from about 4.4-5.7 μm s^{-1} at room temperature to about 10.3–12.9 μm s^{-1} at 70 °C. However, regardless of the substrate temperature, the micro-wires retained a substantial porosity, which was calculated to be between 91.5% and 93.5%. A thermal annealing of 10 min at 180 °C was thus required to consolidate the gold NPs and reduce the specific electric resistivity of the wires to values compatible with their intended application in micro-electronic devices.

In order to tackle the structural weakness of colloidal structures held together by pure van der Waals forces, the technique developed by Domènech et al. [59] was a customised DIW of a colloidal suspension of Fe_3O_4 NPs in toluene, where the ceramic particles were surface-treated with oleic acid acting as ligand. After printing, the organic phase was thermally crosslinked at 325 °C. Obtained geometries were millimetre-long needle-like structures, with a diameter exceeding 100 μm. Under 3-point bending, the elastic modulus of the crosslinked columns varied between 8 and 58 GPa, and the bending strength between 39 and 110 MPa, thus reaching the elastic modulus and strength of natural enamel. Coherently with the Griffith theory, the variability observed in the mechanical properties was attributed to the presence of pores, which were randomly sized and distributed, corresponding to 0.6% of the entire part's volume.

Self-assembled NPs dynamically interacting through non-covalent bonds are ideal candidates for establishing reversible bridges between larger building blocks. For example, traditional hydrogels are very common as cell culture substrates. Nonetheless, they are impaired by the so-called "biofabrication window", whereby increasing the stiffness (for example, by increasing the polymer concentration or the degree of crosslinking) will help improve the printing quality and accuracy, but will also reduce the porosity. The decreased availability of open and interconnected pores may have detrimental consequences for cell viability [62]. Granular microgels, which are made by the packing of hydrogel microparticles, can partly circumvent this issue, since their modular architecture allows stiffness and porosity to be decoupled. Nonetheless, granular microgels only become printable by MEX when they are in the "jammed" state, i.e., when they are tightly packed, or in the "embedded" state, i.e., when they are bound by a viscous matrix. In both cases, inter-granular pores are severely reduced. Ataie et al. [62] reported on a new nanoengineered granular bioink (NGB) that achieves a shear thinning behaviour appropriate for MEX thanks to heterogeneously charged silicate nanoplatelets dynamically gluing together loosely packed gelatine methacryloyl (gelMA) droplets having a diameter of around 80 μm. The nanoplatelet surface is decorated with anionic groups, whilst cationic groups are prevalently located at the nanoplatelet rim. Due to the electrostatic forces, the nanoplatelets spontaneously self-assemble into reversible chain-like structures, which are linked to the functional groups of the polymer chains dangling out from the gelMA droplets. Since the micro-gel granules behave cohesively thanks to the bridging effect of the silicate nanoplatelets, the nanoengineered granular bioink attains or even exceeds the printability of conventional bulk and granular hydrogels. Simultaneously, they preserve the rich porosity of loosely packed microgels, thus optimally supporting cell viability.

Depending on their specific mineral structure and composition, silicate nanoplatelets in the form of clays naturally receive a locally varied electrical charge when dispersed in aqueous media. This is the case, for example, with laponite, a synthetic magnesium silicate clay belonging to the TOT family (namely, each nanoplatelet is composed of an octahedrally coordinated magnesium oxide sheet sandwiched between two tetrahedrally coordinated silica sheets). In water media, sodium and other alkaline metal ions dissociate from the faces of each nanoplatelet, thus making them negatively charged. Conversely, hydroxide ions dissociate from the rim, thus producing a slightly positive charge. Driven by the electrostatic interactions, clay nanoplatelets in aqueous media self-assemble to create a so-called "house-of-cards" arrangement. The resulting colloid exhibits a thixotropic behaviour, because the nanoplatelets disassemble and start to flow easily if the applied shear stress, τ, exceeds the electrostatic interactions, as illustrated in Fig. 3. Once the shear stress is removed, the electrostatic forces are promptly restored, the "house-of-cards" is reinstated, and the suspension transitions back to the self-supporting gel condition [63,64]. Jin et al. [65] noticed therefore that laponite suspensions, on account of their thixotropic (shear-thinning) behaviour, have the potential to be printed by MEX, since the pressure applied in the print nozzle is enough to outbalance the energy required to disrupt the "house-of-cards" structure. After flowing through the nozzle, it takes less than 0.1 s for the "house-of-cards" arrangement to be resumed, thus avoiding any post-printing spread and geometric deformation. Moreover, nanoclays can be mixed with soft hydrogels for MEX and, provided that only physical interactions are established, the composite hydrogels still retain the "house-of-cards" assembly. This has proved to enable the DIW of soft structures that do not need a liquid supporting bath or a post-printing solidification treatment [65].

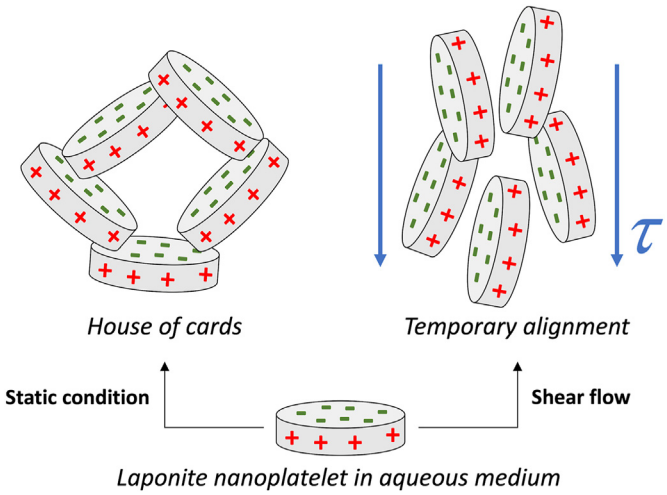

Fig. 3. Laponite nanoplatelets in aqueous media receive a negative charge on their faces, and a positive charge on their rim. Owing to the electrostatic interactions, in a static condition laponite nanoplatelets self-assemble in a "house-of-cards" arrangement (*shown on the left*). However, if the applied shear stress, τ, exceeds the energy required to overcome the electrostatic interactions, the "house-of-cards" structure is disassembled, and the nanoplatelets can easily flow (*shown on the right*). Once the shear stress is removed, the nanoclay suspension quickly reverts to the "house-of-cards" state.

Alternatively, NPs can self-assemble onto the surface of larger particles to be processed as composite feedstock. This principle has been demonstrated, for example, with graphene oxide [66] and MXenes [67,68] for obtaining high-performance metal-matrix composites. MXenes have been receiving great attention in the literature due to their exceptional properties and versatility. MXenes are carbides and nitrides of early transition metals according to the general formula $M_{n+1}X_nT_x$. This means that $n + 1$ (where $n = 1$–3) layers of early transition metals ("M" in the general formula) are interleaved with n layers of carbon or nitrogen ("X"). The "T_x" in the formula represents the surface functional groups bonded to the outer M layers, which can be O, OH, F, and/or Cl [69].

Wyatt and Anasori [67] argued that, due to their surface groups, MXenes exhibit a negative surface charge in water or in polar organic solvents, such as ethanol. Conversely, if not oxidised, aluminium particles become ionised and receive a positive charge in water. After ball milling, the aluminium particles were dispersed in ethanol in order to expose new (non-oxidised) surfaces and to change the shape from nearly spherical to flake-like. Wyatt and Anasori [67] used a mixture of water and ethanol to induce the self-assembly of MXenes ($Ti_3C_2T_X$) onto the surface of the aluminium flakes through electrostatic adsorption. Adding 2 wt% of $Ti_3C_2T_X$ produced the near-complete decoration of the surface of the aluminium flakes with single-to-few layer thick MXene deposits. It was also shown that the fraction of MXene completely adsorbed can be modulated through the positive surface charge of the aluminium flakes,

which depends on the ratio between water and ethanol in the processing solution.

The ability to target the near-complete coverage of aluminium particles with MXene sheets can be exploited to create a continuous network for structural reinforcement and electrical conductivity. Meanwhile, the electrostatic-driven self-assembly process is scalable to form large batches of composite powders, as required for AM [67]. However, whilst the idea of unleashing the potential of MXenes in AM is exciting, some hurdles still remain, such as the conspicuous volumes of fluoride-containing solutions or molten salts that are required for the chemical etching of MXenes from their precursors. Moreover, additional research would be required to ascertain the effect of the MXene adsorption on the flowability and printability of the original feedstock powder, as well as to confirm the survival of the surface decoration through the printing environment and temperature, which are usually very harsh in most metal AM methods. The printability-related issues were explored by Zhou et al. [68], who coated aluminium spherical particles with $Ti_3C_2T_X$ MXene sheets through electrostatic interactions and processed the decorated particles by laser-based powder bed fusion (PBF). With MXene sheets being ultra-thin and flexible, the aluminium particles preserved their original flowability. Moreover, the laser absorptivity of aluminium at the wavelength of the PBF system increased from 49.6% to 67.3% with the addition of 1 wt% of MXene, thus resulting in improved printability. Thanks to their high laser absorptivity, MXene sheets increased the local temperature of the aluminium particles and hence promoted strong Marangoni convection forces. This caused the amorphous alumina layer originallu present on the aluminium particles to break and recrystallise as α-alumina. Meanwhile, the oxygen-containing functionalities of MXene also reacted with aluminium atoms to form α-alumina particles. Whilst most of the MXene nanosheets survived into the printed parts, a minor fraction was dissolved in the molten aluminium matrix, which promoted the nucleation and growth of TiC nanorods.

Lastly, AM parts can be treated after printing to receive new functionality through self-assembly of active NPs. In order to obtain free-standing and binder-free hybrid supercapacitors, Rezaei et al. [70] printed complicated lattice structures by stereolithography (SLA) using a commercial resin that can be pyrolised when treated at high temperature in an oxygen-free atmosphere. With the resin being made of acrylated monomers and methacrylated oligomers, the surface of the AM parts was already rich in functional groups. However, the surface availability of oxygen-containing groups was further increased through oxygen plasma exposure. Next, MnO_x nanoflakes and nanoflowers were deposited on the plasma-treated surfaces via one-step wet chemical reduction of a manganese salt solution (1.25, 2.5, 5, and 10 mM) in HCl. As a result of the wet chemical bath deposition (WCBD), the manganese salt was reduced to manganese oxide, which self-assembled into nanoflakes and ultimately into complicated hierarchical structures resembling carnation flowers when the precursor concentration reached 2.5 mM. The samples were finally treated in an inert environment at 900 °C to induce the pyrolysis of the resin substrates and, simultaneously, to purify, re-orient, and recrystallise the MnO_x nanostructures. The nanoflake and nanoflower features changed to tetragonal structures, whose size and distribution density increased with the concentration of the precursor. For high concentrations, tiny rod-like nanostructures could also be detected on the pyrolised substrates. The fine architecture of the carbon-based lattices, combined with the self-assembled MnO_x nanostructures, led to appreciable values of capacitance, charge-discharge rate capability, and cycling life duration, with the additional advantage of the architectural tailorability enabled by 3D printing.

3.2. 3D printing-enabled SAMAM

The self-assembly of matter may occur through mechanisms that are inherent in the AM process itself (for example, the flow-induced shear stresses existing in MEX). This 3D printing-enabled self-assembly sits therefore at the intersection between spontaneous SAMAM and field-assisted self-assembly, meaning that no external fields are required, but the spatial arrangement of molecules and particles is directed by printing-induced driving forces, and not by pure thermodynamic factors.

In inkjet printing and aerosol jet printing, composite inks consist of insoluble fillers, such as micro- and nano-particles, polymers and biomolecules, suspended in a liquid carrier (often termed “solvent”). Films and functional devices are deposited through the ejection of fine ink droplets from a nozzle (or an array of nozzles) onto a substrate. Upon evaporation of the solvent, the dispersed particles may spontaneously self-assemble in a ring-like pattern called “coffee ring”. This happens when the contact line at the substrate-liquid-air interface becomes pinned. The liquid phase, which preferentially evaporates at the outer rim of the droplet next to the pinned contact line, is continuously replenished by other liquid coming from the interior of the droplet. The established outward flow drags more and more particles and solutes towards the droplet edges, thus generating the characteristic ring. Whilst evaporation phenomena are essential for inkjet printing with solvent-based inks, the evaporation-driven self-assembly of solutes and dispersed NPs can be manipulated or even suppressed to obtain different drying patterns through the appropriate choice of the composition and concentration of the ink, the geometry and size of the particles, the temperature, and the nature and surface properties of the substrate [71,72]. For example, the coffee-ring effect has been reported to aid in the high-resolution printing of microscale conductive lines with strongly aligned CNTs [73]. Conversely, homogenous films characterised by a complete alignment of CNTs can be produced with highly concentrated suspensions, such that the CNT concentration consistently remains above the critical threshold needed for the transition from isotropic suspension to liquid crystal [74].

In MEX, the feedstock, either an ink or a molten thermoplastic-based system, is forced to flow through a nozzle (namely, it is “extruded” - hence the name of this AM family). Shear stresses unavoidably give rise to a preferential orientation of matter along the flow direction. For example, in FFF polymer chain molecules in the molten state and, if present, elongated fillers and fibres receive a strong directionality while flowing through the print nozzle. Though marginally disrupted by die swelling and spreading effects, this preferential alignment along the print direction is largely retained in the printed object. This, coupled with the creation of inter-raster interfaces, explains the difference between longitudinal and transverse direction observed for most FFF parts when testing mechanical and functional properties [75,76]. Whilst this directional arrangement is sometimes regarded negatively as one of the main causes for the in-plane anisotropy of FFF parts, it can be actually leveraged to modulate the mechanical properties of neat polymer parts according to specific load configurations, or to produce pathways for thermal and electrical conductivity in composite parts with a relatively low filler loading [77].

The flow-induced orientation happening in FFF inspired Gantenbein et al. [78] to print hierarchical liquid-crystal-polymer structures that leverage the structural anisotropy of FFF parts to achieve exceptional mechanical properties. Gantenbein et al. [78] observed that, in the molten state, the rigid molecular segment of aromatic thermotropic polyesters self-assemble into ordered nematic domains. If the melt is at rest, the individual domains are randomly oriented. However, when the melt is forced to flow through the print nozzle of an FFF printer, the domains become preferentially aligned in the flow direction. Once the polymer leaves the nozzle, the flow field ceases, and the printed material starts to cool down to ambient temperature. A radial temperature gradient is then established within the printed raster of material. The skin, whose temperature drops down suddenly, retains the preferential alignment of the nematic domains. Conversely, the core cools down slowly and therefore the polymer chains have more time to re-orient randomly due to thermal motion. The printed raster of material ultimately receives a core-shell structure, in which a highly oriented skin surrounds a less oriented core. The relative thickness of the skin with respect to the diameter of the raster can be increased by reducing the

nozzle diameter and the layer thickness. Decreasing the print temperature has a similar effect, since the raster cools down more rapidly. The ability to control the relative thickness of the skin has important consequences on the mechanical behaviour, since the axial tensile stiffness and strength of the raster increase as the skin becomes comparatively thicker [78]. Normally, having this ordered structure at the surface of the printed raster would be a potential disadvantage in FFF, because the reptation mechanisms (namely, the thermally activated motion of polymer macromolecules through an entangled melt) that are responsible for healing the inter-raster surface would be hindered by the strong molecular alignment of the skin, and this would undermine the fusion of neighbouring rasters into a solid part [79,80]. However, the aromatic polyester in the contribution by Gantenbein et al. [78] can be crosslinked via a simple thermal annealing. The post condensation reaction between the end groups of the polymer chains not only increases the average molecular weight, but also promotes crosslinking between adjacent rasters, as demonstrated by the exceptional flexural strength of transverse (i.e., printed by 90° orientation) layers. Interestingly, the hierarchical structures described by Gantenbein et al. [78] demonstrate that, as often seen in biological materials, anisotropy can actually be the key to achieving parts that combine structural strength, lightweight, and (due to the absence of fibres and fillers) recyclability.

An elegant example of biomimetic hierarchical architecture obtained by merging molecular self-assembly and processing-induced forces in MEX is provided by the osteochondral constructs developed by Rajasekharan et al. [81]. The base material is a hexagonally ordered and polymerisable lyotropic liquid crystal (LLC) gel, where di-acrylate modified, amphiphilic triblock copolymers self-assemble into cylindrical and hexagonally ordered nano micellar fibrils (NMFs) having a high aspect ratio (diameter, $d = 10–100$ nm and length, $l = 100\text{-}10\,000$ nm). Under normal processing conditions (e.g., in mould casting), such NMFs are randomly oriented. Conversely, by applying extrusion shear as it happens in MEX, NMFs become preferentially aligned with the flow direction. Crosslinking through the acrylate groups under UV stabilises the acquired directionality. After demonstrating that the nanoscale can be controlled upon printing through shear-enabled self-arrangement of matter, Rajasekharan et al. [81] modified the initial LLC gel by replacing water with a calcium phosphate (CaP) precursor. After 3D printing, the modified constructs were treated with ammonia gas to induce the precipitation of CaP NPss. The highly oriented NMFs acted as a template for the biomineralisation process and tightly wrapped around the newly formed CaP particles. In spite of the absence of a chemical interaction at the interface, the elastic deformation of the NMFs around the particles originated strong contact points. Under compression, the response (stiffness and strength) and failure mechanisms at the macroscale were governed by the interplay of intrinsic features (especially the molecular weight of the starting BCPs and the alignment of the NMFs at the nanoscale) and extrinsic features (micro- and macroscopic architecture dictated by the CAD file for printing). Due to the close resemblance between the 3D printed hierarchical structures and bone tissue, Rajasekharan et al. [81] designed and 3D printed a plug that reproduced the functional gradient of human osteochondral tissue. The device combined a compositional gradient, which was achieved by selectively soaking different areas of the plug in CaP precursor solutions having different concentrations, and a structural gradient, which was produced by developing a printing toolpath that mimicked the natural structural alignment of calcified cartilage and the porosity of subchondral bone. The plug exhibited a graded compressive stiffness that closely matched the behaviour of natural osteochondral tissue. The plug may thus be considered an ideal candidate for replacing conventional synthetic osteochondral devices, since the functional gradient stimulates a local stress redistribution similar to natural bone tissue, and the absence of sharp interfaces avoids delamination between areas having heterogenous mechanical properties [81].

Due to the shear-induced molecular alignment, the ability to absorb water of polymers processed by MEX methods is anisotropic, with swelling being usually stronger in the transverse direction than in the longitudinal one. If exposed to water or to environmental moisture, polymer layers printed under different orientations naturally tend to swell differently, but they are not free to do so because they are mutually constrained by the inter-layer bonding. This forces the printed part to bend and change its shape [4]. This kind of responsiveness, called hygromorphism, mimics the behaviour of flowers and pinecones that are able to open up as a result of water uptake. The shape change can be programmed through the stacking sequence (namely, through the relative orientation of subsequent layers) and the part's geometry. Interestingly, the anisotropy associated with the shear-induced molecular alignment ultimately promotes a complex actuation ability, even if the base polymer *per se* is not a smart material. The shape responsiveness may be strengthened by introducing fillers, like natural fibres, which are anisotropic and sensitive to moisture [82].

Shear-induced alignment is spontaneous in most MEX technologies owing to the laminar flow of fluid that is naturally established while printing through the nozzle. However, shear-induced patterning can also be promoted in VPP thanks to the implementation of a sliding or rotating resin vat. For example, in the contribution by Yunus et al. [83], a linear harmonic oscillator mechanism (i.e., a linear slide connected to a cam which is driven by a stepper motor) acts on the resin tank to generate oscillatory Couette flow.

In the research by Trujillo-De Santiago et al. [84] the laminar flow between two eccentric counter-rotating cylinders is programmed to generate “chaotic printing”. As illustrated in Fig. 4, the printing rig, which is the miniaturisation of an eccentric “journal bearing” flow set-up [85], consists of a cylindrical reservoir (the external cylinder) filled with a viscous polymer resin, and an eccentric shaft (the internal cylinder). A drop of printing ink (which can be a pregel drop, a suspension of fluorescent particles, NPs, or cells) is injected into the resin, and mixed with it by the relative motion of the reservoir and the shaft. The external cylinder is rotated counter-clockwise by a certain angle, then the system is paused for a moment, and finally the internal shaft is rotated clockwise by a certain angle. Applying a low rotation speed for mixing enables the development of laminar flow, and the protocol can be repeated for a number of cycles. As the ink drop is drawn by the laminar flow and mixed into the resin bath, the interface between the ink and the viscous fluid increases and generates a highly convoluted structure, which can ultimately be locked in place by curing or crosslinking. Interestingly, each pattern is unique, because it generates from the chaotic mixing of the two liquids. Nonetheless, this is a controllable chaos, since the length of the stretched ink drop can be precisely predicted as a function of the rotation protocol and the properties of the liquids. In this case, SAMAM leads to a programmable printing of chaos.

Processing-induced self-assembly of matter has also been reported to occur in metal-based PBF. According to Wang et al. [86], metals in laser PBF (i.e., selective laser melting, SLM) experience an unusual thermal history, which is radically different from conventional processing. Metal particles are rapidly heated and melted, and then quenched down with a high thermal gradient. This first thermal input is followed by cyclic heating-cooling during the deposition of additional layers. The non-equilibrium conditions associated with the interaction between the metal and the incident beam produce tension-compression cycles in the solidified part, which are responsible for the nucleation and self-assembly of dislocations. Driven by these periodical stresses, dislocations glide back and forth, which annihilates unstable dislocation dipoles and promotes the establishment of Lomer locks (a.k.a. Lomer-Cottrell junctions [87]). Since Lomer locks are sessile and immobile in the slip plane, they act as a barrier preventing other dislocations from moving in the plane. The self-organisation of dislocations into an inter-pinned configuration provides metal parts produced by laser PBF with exceptional mechanical properties and overcomes the strength-ductility trade-off generally encountered with conventional processing methods. Moreover, the dislocation pattern can be manipulated in situ through the printing parameters, thus enabling the

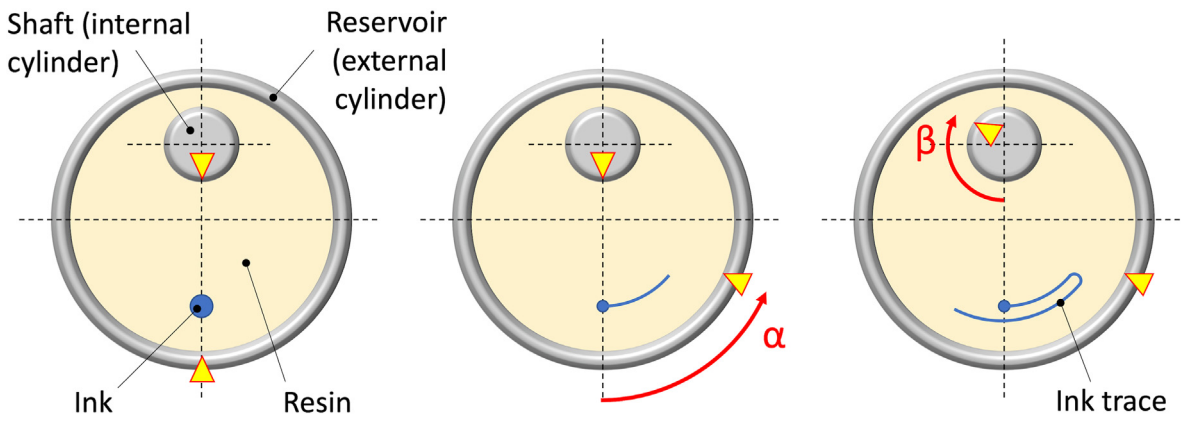

Fig. 4. In the experiment conducted by Trujillo-De Santiago et al. [84], a drop of ink is injected into a viscous resin bath. Then, the reservoir (external cylinder) is rotated counter-clockwise by a certain angle α, the system is briefly paused, and finally the eccentric shaft (internal cylinder) is rotated clockwise by a certain angle β. The ink is progressively drawn by the laminar flow and mixed into the resin to create a highly convoluted pattern.

achievement of self-strengthened parts in the as-built state, without any additional post processing (process intensification) [88].

3.3. Field-assisted SAMAM

In order to locally govern the microstructure of composite systems, AM can be coupled with external fields (for example, magnetic, electric, or acoustic fields) that affect the local concentration, distribution and (mostly for elongated or flat particles) the orientation of the filler in the matrix [30]. Whilst the action of external fields is an established means of inducing the directional assembly of fillers in conventional polymer processing [89], the combination of external fields and AM is a new concept, presently referred to as "field-assisted" or "field-aided" AM (FAAM).

3.3.1. Magnetic FAAM

For magnetic FAAM to be effective, the filler must be magnetically active. In this regard, particles can be entirely made of a magnetically active material; otherwise, thanks to magnetic labelling techniques, magnetically active NPs can also be clustered on the surface of larger nonmagnetic substrate particles.

Materials can exhibit different kinds of magnetic activity. Diamagnetic materials are repelled, though very weakly, by magnetic fields. The effect is transitory, as it just persists as long as an external magnetic field is applied. For example, water is a diamagnetic material [90]. Paramagnetic materials like aluminium and platinum become magnetised if subject to a magnetic field, but their magnetism disappears when the field is removed. In paramagnetic materials, atoms, molecules, or ions possess a magnetic dipole moment, but in absence of an external magnetic field the dipole moments are oriented randomly and therefore there is not net magnetisation at the macroscale [91,92]. In ferromagnetic materials, as a consequence of long-range ordering, magnetic dipole moments are aligned within regions called domains. Each domain generates a relatively strong magnetic field, but domains are randomly oriented and therefore the net magnetisation at the macroscale is zero. However, even a relatively small external field is sufficient to line up the magnetic domains, and the material is then said to be "magnetised". Due to a phenomenon called "hysteresis", ferromagnetic materials can retain to some extent their magnetisation once the driving field has been removed [91,92]. Besides iron, cobalt, and nickel, also many spinels (e.g., cubic magnetite, Fe_2O_3·FeO) are ferromagnetic materials [92]. If a magnetised ferromagnetic material is able to retain most of its magnetisation at zero driving field, the material becomes a permanent magnet. Good examples of permanent magnets with a strong residual magnetisation are ternary compounds in the NdFeB family ("neodymium magnets" [93]).

For a given material, magnetic properties are size-dependent, as demonstrated, for example, by ZnO. Whilst ZnO is a nonmagnetic oxide, ZnO NPs can be in the ferromagnetic state due to "defect-induced magnetism" (DIM) as a result of the exchange interactions occurring between surface defects such as Zn vacancies. Whilst these interactions are negligible in bulk materials, they are amplified by the huge specific surface area of NPs [94]. When ferromagnetic NPs are extremely small and their diameter is below 3–50 nm (depending on the material), each NP can be assumed to behave like a single magnetic domain. Due to the effect of temperature, the magnetisation of these single-domain NPs can flip randomly, with the average time between two flips being called "Néel relaxation time". In absence of an external field, if the time required for measuring the magnetisation of the NPs largely exceeds the Néel relaxation time, on average the net magnetisation appears to be zero. This behaviour is known as super-paramagnetism [95]. Temperature is also very important. If heated above the Curie point (a.k.a. Curie temperature), a ferromagnetic material loses its properties and becomes paramagnetic. This happens because the energy associated with thermal vibration becomes sufficient to overcome the internal forces that, at low temperature, keep the magnetic structure ordered within the individual domains [92].

Magnetic FAAM with paramagnetic fillers or with diamagnetic fillers decorated with paramagnetic NPs is the preferred choice whenever the driving magnetic field serves to achieve a complicated structural pattern while printing, but magnetic activity is not necessary for the final use. For example, Kokkinis et al. [96] fabricated objects with exquisite microstructures using alumina platelets decorated with super-paramagnetic iron oxide (magnetite) NPs as the magnetically responsive filler. Based on previous research, the size of the decorated alumina platelets was accurately chosen in order to minimise the time required for rotating under the magnetic field, while reducing the detrimental effect of thermal energy (that causes randomisation) and force of gravity (that causes precipitation). The ultra-high magnetic response (UHMR) corresponded to an average diameter of 5 μm [97]. The sophisticated experimental set-up comprised a multi-nozzle DIW printer, a rotating magnetic field generator and a mask-assisted photocuring unit. For each layer of the structure, the outer perimeter was printed with a viscoelastic structural ink to define the contour of the 3D geometry. The interior was filled with the alumina-functionalised composite ink, whose rheological behaviour was controlled through the addition of fumed silica. A magnetic rotating field was first applied to align the platelets in one specific direction, and the obtained pattern was consolidated in selected areas through mask-assisted photocuring. The magnetic alignment was then changed and locally consolidated again. The patterning/photocuring workflow was repeated until completion of the desired microstructure for that layer. Compositional gradients, if required, were introduced by changing

the filler loading in a static mixer just prior to extruding through the DIW nozzle, and additional geometric complexity was enabled by sacrificial support materials. Kokkinis et al. [96] also observed that, in composite layers with ordered alumina platelets, swelling of the polymer matrix in a liquid medium preferentially occurred in the direction normal to the platelets. As a proof of concept, this anisotropic absorption of liquids was harnessed to produce a controlled bending of the matching surfaces of a 3D printed smart key-lock connector.

In the contribution by Martin et al. [98], magnetic FAAM of diamagnetic particles decorated with magnetically active NPs was also demonstrated with digital light processing (DLP) photopolymerisation. Conceptually, the workflow was similar, since printing each layer required repeating the patterning/photocuring steps area by area. First, the decorated filler was lined up under the external magnetic field, and the resin bath was locally photocured in those voxels that should retain that specific orientation. Then, the magnetic field was shifted to change the filler alignment, and the areas corresponding to the new orientation were crosslinked to fix that orientation. After photocuring all areas in a single layer, DLP printing proceeded with the addition of the subsequent layer. However, unlike the procedure developed by Kokkinis et al. [96], the magnetic-assisted DLP system proposed by Martin et al. [98] did not require printing a structural material to define the part's contour. A simple composite resin containing magnetically-decorated platelets enabled the design of complicated hierarchical structures mimicking the different reinforcement distribution observed in natural heterogenous materials including the nacre-like shells of abalones, the dactyl club of the peacock mantis shrimp, and the concentric arrangement of plywood structures in mammalian cortical bone. Patterning isolated regions having a contrasting orientation to the surrounding material made it possible to control and steer the crack propagation in the printed parts, with cracks being turned away by islands having 0° orientation in a 90°-oriented material, and being attracted towards islands having 90° orientation in a 0°-oriented material.

Conversely, ferromagnetic fillers, in addition to their patterning capability, can provide the printed part with a certain degree of permanent magnetisation, which can be leveraged for liquid-free magnetic-actuated 4D printing. For example, Nakamoto and Marukado [99] combined an SLA printer with an array of five electromagnets (one vertical and four horizontal) that generated a tunable magnetic field on the resin vat. Ferromagnetic fibres were dispersed in a commercial photocurable resin, and then progressively lined up while printing layer by layer. Once finished, the printed part was magnetised by applying a driving field parallel to the fibres' axis. In this way, the residual magnetic flux density in the direction of the aligned fibres was maximised, and the part could be easily actuated by a permanent magnet, and induced to bend remotely without physical contact. Moreover, the shape change was triggered without swelling the structure in a liquid, as commonly observed in 4D printed hygromorphs.

The morphing ability is emphasised when ferromagnetic fillers are dispersed in a soft and flexible polymer matrix, as demonstrated by the complicated smart structures programmed by Kim et al. [100]. Magnetisable microparticles of neodymium alloy as the active filler and fumed silica NPs as the rheological modifier were embedded in a silicone rubber matrix to obtain an ink printable by DIW. The neodymium alloy filler was magnetised, and then oriented upon printing by means of a controllable magnetic field coupled with the print nozzle. With the guidance of finite element simulations, planar shapes with extremely complicated patterns of differently oriented ferromagnetic domains were printed, and then magnetically actuated to obtain artistic 3D geometries and auxetic metastructures. The flexible polymer matrix was key to enabling fast and fully reversible folding and unfolding under remote magnetic actuation. More complicated 3D parts were also printed with the aid of a washable support material. Curiously, the 3D auxetic structure was so responsive as to "jump" after a sudden reversal of the applied magnetic field, thus generating a leap forwards of 120 mm on the horizontal plane within 0.7 s.

Although magnetic FAAM is theoretically feasible with all techniques capable of printing a composite material with a liquid matrix, magnetic patterning is most frequently combined with VPP, owing to the relatively straightforward reorientation of the filler in the resin bath, which is then retained through the curing stage [30]. However, a potential drawback may come from the interference between the filler and the incident light, as the particles may cause shadowing or scattering effects, thus preventing the resin from curing completely, reducing the beam penetration depth and impairing the print resolution [101].

3.3.2. Electric FAAM

Electric fields are at the core of an emerging area of additive nanomanufacturing known as electrohydrodynamic (EHD) printing. A voltage is applied between a nozzle (also serving as electrode) and a collector (also working as counter-electrode) to induce the ejection of ink either in the form of a continuous fibre (electrospinning [102,103]) or in the form of individual sub-micrometre droplets (electrohydrodynamic inkjet (e-jet) printing [104,105]). Fibres and droplets can then be assembled into more complicated 3D structures [106,107].

In addition to electrohydrodynamic printing, electric fields, much as magnetic fields, can be combined with other AM technologies in order to produce a programmed reinforcement orientation. In electric FAAM the filler's particles must be sensitive to an electric field. Particles can be either conductive, in which case they experience charge separation, or dielectric, in which case they become polarised [108]. Electric fields can stimulate different patterning mechanisms, for example by changing the charged state of electrically active NPs, promoting electrostatic interactions, or triggering thermal effects [25]. As a result, fillers in electric FAAM can thus receive a preferential orientation to affect a controlled anisotropic response to mechanical loads or, more often, to generate a percolation pathway for thermal and electrical conduction [108,109]. After electrical stimulation, if the filler concentration is high enough, smaller particles can be aligned to form larger pseudo-fibres that are lined up with the direction of the electric field [108].

As already seen for magnetic fields, VPP dominates in the literature regarding electric FAAM, owing to the relatively fast filler's motion in the low-viscosity resin. For example, Holmes and Riddick estimated that the resin's viscosity should be lower than 1000 cP for alignment to take place in seconds when aluminium particles having an aspect ratio close to 1 and a diameter in the 20–50 μm range are to be actioned [108]. The rheological properties of the resin should be adjusted to compensate for the thickening effect of adding a filler. Moreover, the presence of the filler may prevent the resin from curing completely due to the undesired interactions with the incident light. An additional complication in electric FAAM comes from the formulation of the matrix, because the resin must be non-conductive in its pre-cured state. Whilst the greatest part of liquid monomers are not conductive, photoinitiators typically are. Since a relatively high concentration of initiator may be required to outbalance the impairing effect of the filler on curing, the mixture of the initiator and the monomer may ultimately become conductive. For this reason, custom-made resins may be needed for successful electric FAAM [108].

A special instance of electric FAAM is represented by MEX (especially FFF) printing under an electric field applied between the nozzle and the base platform to induce the poling of polyvinylidene fluoride (PVDF) macromolecules. In this case, the action of the electric field is exerted directly on the polymer chains, and not on the filler. The basic goal of poling is to favour the development of the (thermodynamically unfavourable) β phase possessing important piezoelectric properties and orient it [110]. The poling effect and consequent piezoelectric properties can be emphasised by the addition of fillers [111].

3.3.3. Acoustic FAAM

Unlike magnetic and electric fields, acoustic fields do not require any specific properties for the filler to be responsive. In other terms, acoustic forces are "material agnostic", meaning that, in principle, they can be applied to any materials, although the specific effects produced by

acoustic forces do depend on the proprieties of the filler (speed of sound, acoustic damping, etc.). Acoustic FAAM is particularly advantageous for bioprinting and other biomedical applications, since it avoids the potential toxicity of magnetic materials and the generation of heat associated with electric fields due to Joule heating, which may have detrimental effects on cell viability [112,113]. Meanwhile, acoustic fields enable a close control over the filler distribution, with the main effect being the migration ("acoustophoresis") of the reinforcement to selected areas of the printed part corresponding to the nodal or antinodal regions of the wavefield [4,30]. The resulting pattern can be coordinated through the properties of the constituent phases, most notably through the "acoustic contrast factor", which expresses the relationship between the density and the compressibility (namely, the speed of the sound) of the fluid and the filler. The sign of the acoustic contrast factor is very important, as it dictates where the particles will converge. If the acoustic contrast factor is positive, the solid particles will migrate towards the pressure nodes (displacement antinodes); conversely, if the acoustic contrast factor is negative, the particles will migrate towards the pressure antinodes (displacement nodes) [114].

The accuracy of patterning depends on the applied wavelength and the average particle size. Typically, bulk acoustic waves (BAWs) have a relatively low frequency below 10 MHz, as opposed to surface acoustic waves (SAWs) that oscillate at a frequency in the range of tens to hundreds of megahertz [4]. Acoustic waves at higher frequency have a shorter wavelength, which is required for attaining tight spatial resolution [115]. Meanwhile, the acoustic radiation force, which is responsible for turning the particles away from the acoustic source, is proportional to the particles' volume [116]. This relationship between driving force and particle size, together with the stronger Brownian motion (in this regard, it is worth mentioning that particles larger than 1 μm do not experience a significant Brownian motion [117]), makes smaller particles more difficult to direct.

It has been argued that, in spite of being capable of a precise distribution of the solid phase, acoustic waves are less appropriate for rotating and aligning the filler's particles [30]. For elongated fibre-like particles, the filler's response depends on the ratio between fibre length and applied wavelength. For example, Yamahira et al. [118] mathematically and experimentally proved that polystyrene fibres dispersed in an aqueous sugar solution are pinned at the pressure node and oriented normal to the direction of wave propagation if they are shorter than one-fourth of the wavelength. Conversely, fibres ranging from one-fourth to one-half of the wavelength can be either parallel to the direction of wave propagation at the pressure loop, or perpendicular to the direction of wave propagation at the pressure node depending on their initial positions and directions. In VPP, if two acoustic tweezers are mounted normal to each other by the sides of the resin tank, the orientation of the fibres can thus be changed mid-print, such that orthogonally aligned layers can be sequentially stacked in the printed part [119]. Spherical particles can also be brought to spin under the action of two standing acoustic waves arranged perpendicularly [120].

Quite often, acoustic FAAM is applied to bulk volumes of liquid resin, mainly in VPP. Nonetheless, the effectiveness of acoustic FAAM has also been demonstrated in DIW. Printing through an "acoustic nozzle" allows the shear-flow induced alignment of the filler to be combined with multi-node acoustic focusing, whereby particles converge to acoustically focused lines [121].

Owing to the low attenuation of acoustic (especially ultrasound) waves in liquid media, acoustic fields are effective over a wide range of resins, regardless of their viscosity. Nonetheless, the drag force that opposes the particles travelling under the action of the wavefield is linearly proportional to the dynamic viscosity of the fluid, which may hamper the migration through highly viscous liquids [122].

4. Discussion

Demoly and André [123] recently discussed the thought-provoking question: "Is order creation through disorder in additive manufacturing possible?". The contribution by Demoly and André [123] investigates whether it is interesting (and reasonably feasible) to exploit available knowledge in spontaneous self-assembly of matter in order to create an object of desired shape, as opposed to AM meant as the "determinist principle of spatially localized material transformation". According to the authors, the reproducible fabrication of macroscale objects merely through spontaneous self-organisation of matter still appears to be unfeasible, "as we are dealing with an insufficient mastery of systems" and "we find [that] the dream of having the universal assembler that could make any object (or organism) from atoms/molecules/voxels taken from the environment" is presently unattainable [123]. However, according to Demoly and André [123], the morphogenetic approach to programmable matter can already be successfully combined with AM, since self-assembly of matter can be locally induced for the realisation of voxels (namely, of transformed elementary volumes) that are the building blocks for AM. In other words, whereas replacing AM with self-assembly of matter for the fabrication of real-life objects is still a visionary goal, merging top-down and bottom-up approaches through SAMAM is a reality.

The perspective article published in 2011 by Crane et al. [8] already delineated some key challenges in SAMAM that are still current. Firstly, the likelihood that a successful bond is spontaneously established between the building blocks in self-assembly becomes very low when multiple elements have to be combined simultaneously. Likely, this is the reason why SAMAM is mainly limited to mono-material systems, or to multi-material systems in which only one type of building block is actually involved in self-assembly. Secondly, when self-assembly occurs at the nano- and micro-scale, a major obstacle comes for the extremely low yield for the fabrication of large assemblies. This issue is most clearly seen when the AM process itself is completed through the self-assembly of individual molecules or NPs (namely, when SAMAM verges on pure self-assembly of real-life devices) as reported, for example, by Tan et al. [60], by Domènech et al. [59] and by Hamoudi et al. [46]. This is why nanoscale functional particles like graphene oxide and MXenes are preferentially decorated on the surface of larger particles that are used as the real building blocks (feedstock) for the AM of macroscale structures [66–68].

Another point to consider is that, in self-assembled functional devices (for example, a hypothetical thermoelectric device in the contribution by Crane et al. [8]), errors in the assembly process can undermine the performance of the assembled system as a whole. Provided that the misplacement of an individual molecule or particle does not trigger a domino effect leading to major printing faults, the correct positioning of each nano- or micro-scale building block seems less critical in SAMAM than it is in purely self-assembled functional components. However, partitioning the assembly into smaller sub-assemblies may help mitigate the impact of assembly errors on the part's performance, in addition to increasing the fabrication yield. The action of external fields may also be leveraged to guide and speed up the migration of matter, driving the building blocks or the functional fillers to the right location within the AM part and increasing the assembly rate.

Crane et al. [8] also identified the difficulty of designing a self-assembly system to reproduce an arbitrary geometry as a possible impediment to SAMAM. This may likely depend on the AM method and the self-assembly mechanism in play. For example, in the contribution by Domènech et al. [59], free-standing millimetre-sized columns were successfully obtained through the direct-write colloidal assembly of individual NPs. However, this required a very fine adjustment of the printing set-up, as the substrate had to be moved downward at a rate perfectly corresponding to the vertical growth rate of the self-assembled needle-like part. As such, the achievement of more complicated, non-columnar geometries or larger scale objects may represent a challenge. Conversely, the design of granular bioinks with reversible interfacial NP self-assembly in the research by Ataie et al. [62] was the turnkey to enabling the bioprinting of scaffolds with interconnected microporosity

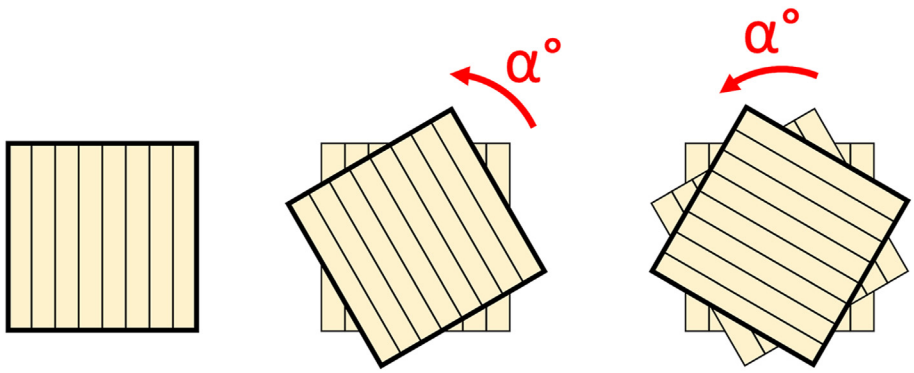

Fig. 5. A Bouligand structure features a layered hierarchical architecture in which reinforcing fibres are rotated by a certain angle, α°, layer by layer. Field-assisted additive manufacturing (FAAM) can mimic Bouligand structures if the applied field is progressively rotated upon printing the individual layers.

and high printing accuracy, which otherwise would be unfeasible with standard bioinks. Coherently with the arguments presented by Demoly and André [123], the geometric feasibility likely becomes more limited as SAMAM approaches pure self-assembly of macroscale objects. Interestingly, in this regard Elder et al. [4] reasoned that the geometric complexity of AM parts, if aided by nano-patterning, is actually fundamental for achieving hierarchical multiscale constructs mimicking those observed in nature. For example, the tightly controlled porosity of AM lattices can be programmed to reproduce the spongy structure of trabecular bone, but this would be impossible with conventional fabrication methods [124]. Likewise, AM can fabricate articulated modular constructs in a single step, thus avoiding the need for joining the individual components after producing them, which often poses cumbersome design constraints in traditional technologies [125]. Self-assembly adds the exquisite features of nanoscale-patterning to this macroscale geometric complexity.

Research in SAMAM predominantly concentrates on polymer-based systems, whilst the contributions targeting metal-based AM are still extremely rare. This discrepancy has historical reasons, since polymer-based SAMAM may tap into the extensive knowledge garnered in the past in regard to the self-assembly of polymers, including the development of supramolecular polymers and the manipulation of covalent crosslinking. Moreover, there appear to be technical motivations for this gap, since the extremely turbulent conditions occurring locally in most metal-based AM procedures are not suitable for accommodating and retaining the self-assembly of matter.

Preliminary research has demonstrated that the printing parameters in metal-based AM can be finely tuned to govern the spatial distribution of nanostructural features such as dislocations [88]. Nanofillers can be added ex situ or grown in situ to promote grain refinement while printing [126]. Similarly, FAAM has been successfully implemented to modify the grain morphology, refine the grain size and displace potential entrapped gas bubbles in neat metal and alloy parts [127–130]. However, much attention has been paid so far to field-assisted directed energy deposition (DED), whilst the integration of external fields with powder bed fusion technologies still remains very challenging because the closed build chamber drastically limits the room available for installing supplementary equipment [112].

Otherwise, self-assembly can help produce composite powders for metal-based AM. The self-assembly of nanofillers on the surface of larger metal particles mitigates the agglomeration issues that are commonly encountered with conventional hybrid methods for producing metal-based nanocomposite powders, such as high energy ball milling. Moreover, loose NPs may easily become airborne. Their prior adhesion to larger particles acting as carrier may thus help prevent process instabilities [131]. Besides introducing new functionality, uniformly dispersed nanofillers can selectively promote nucleation events, stimulate the columnar-to-equiaxed structure transition and favour grain refinement [22,24,67,68]. NPs have also been reported to mitigate the formation of keyhole pores in laser-based metal AM [132].

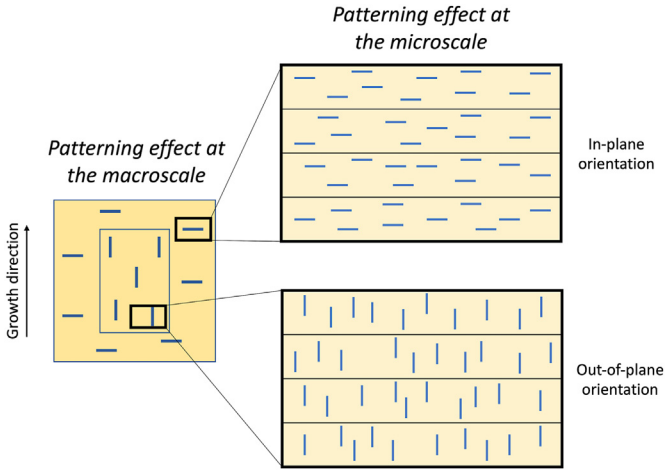

Fig. 6. Field-assisted additive manufacturing (FAAM) can produce parts that feature a preferential alignment of the filler parallel to the growth direction. However, fillers are patterned and fixed in place within individual layers, and therefore they cannot bridge the layer interface.

According to the broad definition of self-assembly as the "spontaneous arrangement of matter to create an ordered pattern", a wide range of opportunities for SAMAM with metal AM may open up through the design of new alloys and multi-elemental systems. For example, eutectic high entropy alloys combine the exceptional ductility and resistance to hot cracking of high entropy alloys (HEAs) with the ability to quickly solidify upon cooling and naturally generate a periodic lamellar structure in which the inter-lamellar spacing can be programmed through the temperature profile [133].

As compared to metal 3D printing, polymer-based AM is more flexible, and offers a spectrum of opportunities for SAMAM beyond the formulation of new self-assembly-assisted feedstock materials. For example, VPP techniques are ideal for supporting self-organisation (directed assembly) through the straightforward transport of matter in a liquid medium under the action of external fields. In MEX, shear forces naturally produce a preferential orientation along the flow direction, which can be leveraged to control the alignment of polymer chains and fillers. Although often regarded as a disadvantage because of its anisotropic effects [134,135], this directionality reproduces natural constructs like brick-and-mortar nacre and thus discloses new functionality like exceptional toughness through crack deflection [136,137].

Among all MEX methods, DIW has received special attention in the literature. On the one hand, DIW, a. k.a. "micro-extrusion", is capable of working at the sub-millimetre scale, and hence naturally lends itself to

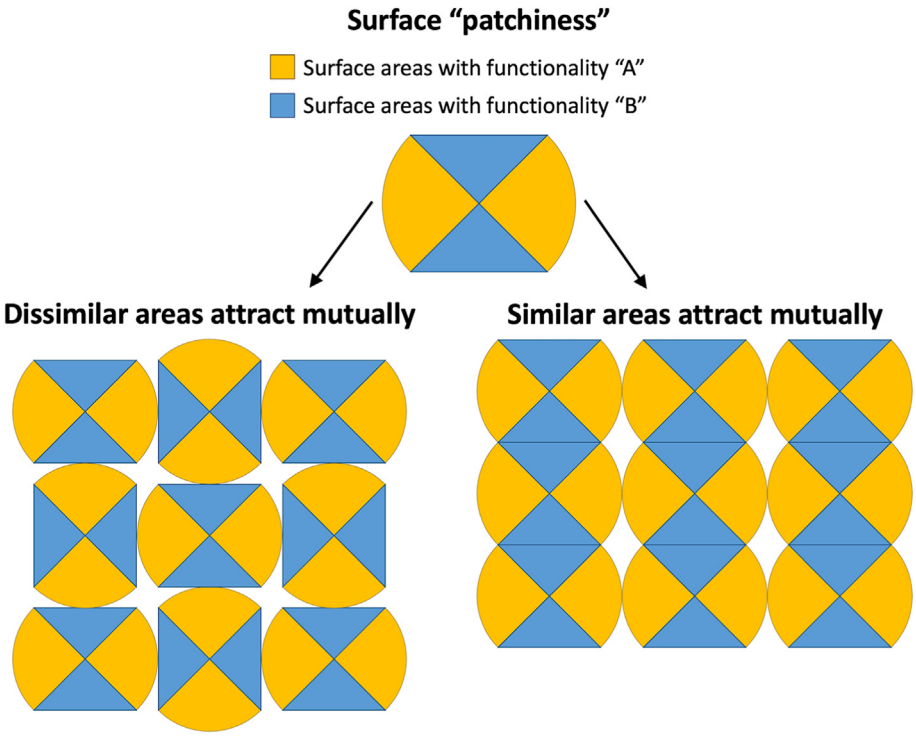

Fig. 7. In a simplifies demonstration of surface patchiness, surface areas of the same NP possess different functionality (i.e., functionality “A” and functionality “B”). NPs can thus self-assemble in different structures if dissimilar areas attract mutually (this is the case, for example, of surface areas having different electrostatic charges) or if similar areas attract mutually (this is the case, instead, of surface areas having hydrophobic and hydrophilic behaviour).

micro-structuring [138]. On the other hand, DIW is extremely versatile, such that it has been ranked as the most flexible AM technique, being able to process the broadest range of materials. This makes DIW the ideal testbed for experimenting with new feedstock materials [139].

Meanwhile, there is an urgent need for improving already existing materials for DIW, especially for producing soft and flexible structures, which are in demand for soft robotics [140] and tissue engineering scaffolds [141]. In order to avoid sagging, the printed structure must be rapidly solidified. For example, thermally sensitive materials can be heated upon printing and then rapidly cooled down after printing in order to trigger their re-solidification. Otherwise, ion-reactive hydrogels can be exposed to ionic solutions, and photocurable resins can be

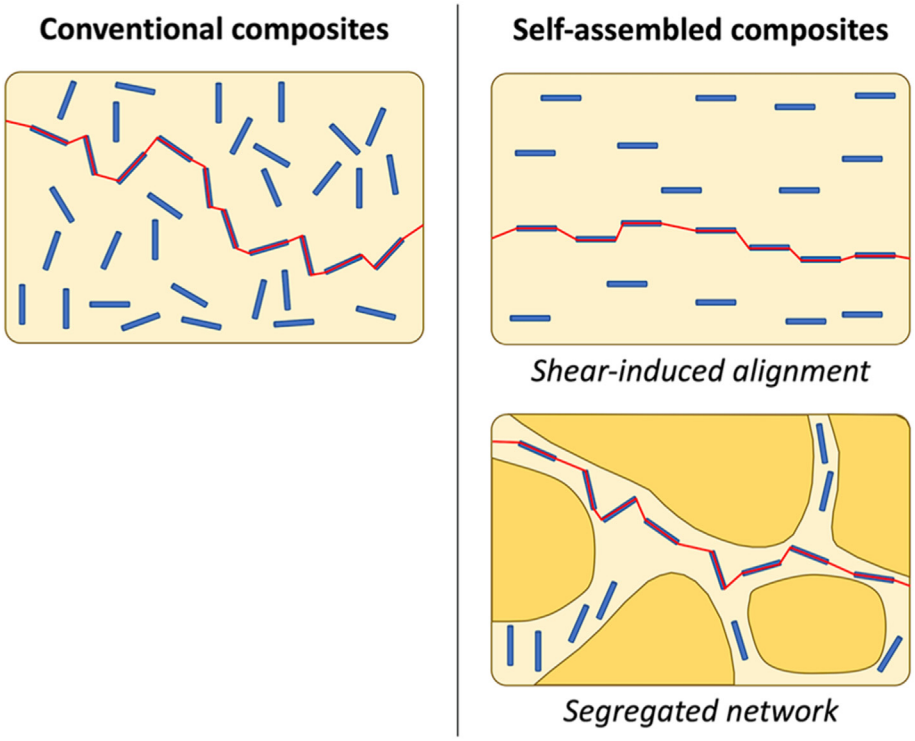

Fig. 8. Schematic representation of the percolation threshold for electrical conductivity in polymer-matrix composites. The volume fraction of filler required to establish a conductive path is higher in conventional composites (shown on the left-hand side) than in self-assembled ones (shown on the right-hand side). In self-assembled composites, fillers can be preferentially aligned as a consequence, for example, of shear stresses (top right), or arranged in a segregated network (bottom right). In this example of segregated network, the filler is segregated in the continuous phase of a sea-island immiscible blend of polymers.

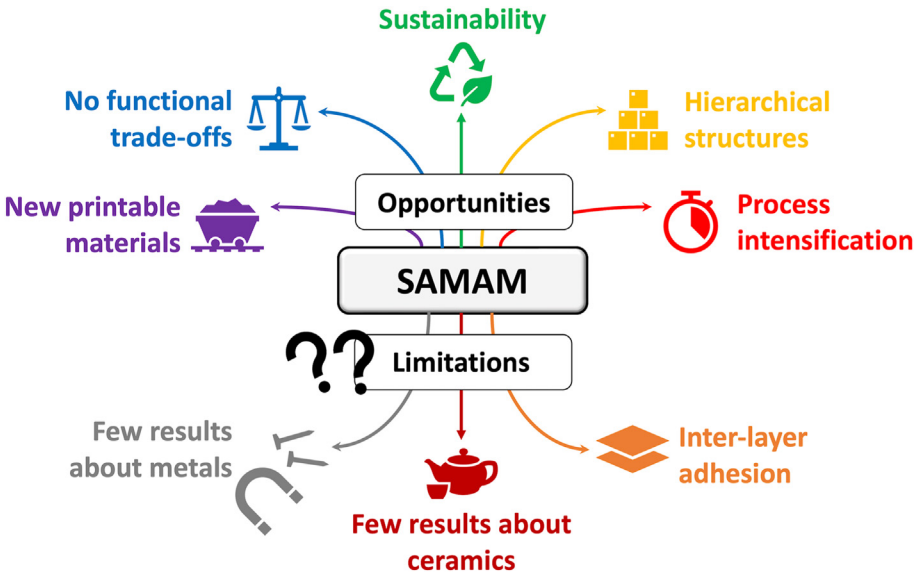

Fig. 9. Graphical outline of the main opportunities and limitations related to SAMAM.

crosslinked under UV light exposure. However, this approach narrows down the selection of available materials for printing, and also limits the geometric freedom due to the absence of supporting structures. As an alternative, soft structures can be printed in a supporting bath. However, the interface between extruded material and supporting bath may be weak, thus compromising the structural integrity of the construct. Quite often, the post-printing removal from the supporting bath is unpractical. This explains the attention being paid in the literature to the formulation of new printable soft inks [65].

In future, it would be interesting to understand if the numerous results reported on SAMAM with DIW can be somehow translated to other MEX techniques. For example, the standard diameter of the print nozzle in FFF is 400 μm. Even if smaller nozzles have been implemented for research purposes, it is currently impossible to target any features smaller than 150–180 μm through hardware-based solutions [142]. As such, a material-based approach to nano- and micro-structuring can be the game-changer for extending the capability of this technology.

If SAMAM is achieved through the spontaneous self-assembly of feedstock materials and through forces inherent in AM, the self-assembly of matter and the part's build-up are coupled. Conversely, FAAM makes it possible to separate the printing process and the microstructural design. In principle, this would endow materials developers with more freedom in controlling the spatial composition of the system and the selective distribution of the filler, and would also ensure that the printing process is not hampered by the presence and self-organisation of the new microstructure [119,143]. Kokkinis et al. [96] defined the FAAM of multi-material (composite) materials as a multi-dimensional design space, where the ability to locally determine the composition (+1D) and to independently vary the filler distribution and alignment (+1D) add on two extra dimensions to the 3D space of AM geometries.

On the other hand, one of the main limitations with FAAM is that, due to the layer-wise build-up of 3D parts, manipulating the orientation of the filler's particles within individual layers in the X–Y plane is relatively simple, but triggering the self-organisation along the third direction is still technically challenging [25,30,32]. The build platform can be rotated by 90° upon printing each new layer. This induces the filler's particles to group along straight lines with a 0°/90° alternating stacking sequence, and the obtained printed part can be regarded as an interpenetrating-phase composite (IPC) even if, strictly speaking, the reinforcement is not continuous. This ultimately results in a so-called "discontinuous IPC" [122]. The orientation of the reinforcement can also be changed layer-by-layer by a smaller angle [144], thus mimicking the hierarchical 3D architecture of Bouligand structures most often seen in crack-resistant biological materials [145,146], which is illustrated in Fig. 5. Nonetheless, the fibres still lay down flat within each single layer.

Tests have been conducted to encourage an out-of-plane through-thickness orientation in VPP thanks to electrical fields acting parallel to the growth direction. To this aim, the build platform itself works as electrode, and aligns the filler's particles vertically within selected areas of each layer. The coordinated repetition of the process layer-upon-layer results in through-thickness alignment at the macroscale [108]. Similarly, elongated fillers can be oriented out-of-plane (i.e., parallel to the growth direction) in magnetic FAAM, in order to produce 3D islands having a different orientation with respect to the surrounding material [98]. Nonetheless, despite fillers being oriented parallel to the growth direction, they remain confined within the individual layers, and therefore they are unable to provide structural continuity across the layer interface, as explained in Fig. 6.

Remediating the relatively weak interlayer bonding, which is often acknowledged as the main cause of the structural deficiency along the growth direction, represents a major challenge in order to enable the safe adoption of AM parts in load bearing applications. This justifies the increasing attention being dedicated in the literature to new printable materials that provide an efficient inter-layer healing, such as the crosslinking polymers proposed by Gantenbein et al. [78]. New fabrication protocols are also emerging, such as the combination of AM and freeze-drying developed by Zhang et al. [147]. In this case, multi-material structures consisting of a water-based graphene oxide ink as the structural material and neat water as the support material are 3D printed by DOD on a cold sink at −25 °C. Every time a new layer is added on top of the previous one, the frozen surface largely remelts. The new material mixes with the previous one, and quickly solidifies under the extremely low temperature of the substrate. In this way, the layer-layer interface disappears. After printing, the object is immersed in liquid nitrogen, freeze dried to remove the water, and thermally annealed to reduced graphene oxide. During the freeze-casting step in liquid nitrogen, the graphene oxide sheets are pushed back and concentrated at the ice crystal boundaries, where they orderly stack through π-π interaction. Since ice crystals grow across the whole architecture, grouping and cross-linking of graphene oxide sheets occur within layers and between layers, thus greatly contributing to structural continuity.

According to Whitesides and Grzybowski [9], self-assembly can be either static or dynamic. In static self-assembly, systems spontaneously evolve to reach and then stay at global or local equilibrium. As such, the

Table 2
Examples of experimental research in SAMAM through local interaction mechanisms (listed according to the in-text reference number as shown in the last column).

Technique	Material	Printed objects	Outcomes	Applications	Reference	No.
Selective laser melting	(3-aminopropyl) triethoxysilane (APTES)-modified AlSi10Mg microparticles electrostatically decorated with tetramethylammonium hydroxide (TMAH) modified TiC nanoparticles	Millimetre-scale specimens	Increased tensile strength and Vickers hardness from grain refinement, grain boundary strengthening, and dispersion strengthening	Extending the capability of metal AM	Fan et al., [2021]	[22]
Selective laser melting	Aluminium alloy (7075, 6061) micro-particles electrostatically decorated with hydrogen-stabilised zirconium	Macroscale testing specimens	Increased tensile strength from equiaxed and refined grain structure	Extending the capability of metal AM	Martin et al., [2017]	[24]
Material extrusion (injection through contact angle nozzle)	Dithiol molecules self-assembled into monolayers with metal ions working as mediators for inter-layer bonding	Nanosheets and rods	Self-healing through the mediation of metal ions at the interface between self-assembled monolayers	Revision of lithographic technology through molecular-level printing: AM parts with self-healing properties	Hamoudi et al., [2022]	[46]
Direct ink writing	Low molecular weight gels (supramolecular polymers)	Comb-like parts bi-layered scaffolds	Soft scaffolds through non-covalent bonds	Soft cell culture, e.g. neurons	Andriamiseza et al., [2022]	[52]
Material extrusion through microfluidic device	Ketone homopolymer self-assembled into nano- and micro-gels and fibres through covalent crosslinking	Basic porous geometries	Size of hydrogels tuned through crosslinking rate	Drug delivery and tissue engineering	Bai et al., [2022]	[53]
Injection-based liquid-in-liquid printing combined with UV curing	Water solution containing amphiphilic molecules (surfactant), pre-polymer and photoinitiator, injected into polar oil medium	Soft helicoid structures, planar constructs, 3-layered scaffolds	Tensile properties increasing with crosslinking density	Synthetic biomaterials that mimic living tissue	Honaryar et al., [2021]	[54]
Stereolithography (prospective)	Methacrylate photocurable resin + block copolymers	No printing	Toughness depending on crosslinking and on block copolymer content	Dentistry	Demleitner et al., [2022]	[55]
Material extrusion combined with UV curing + drying and sintering	Bioactive glass sol + acryloylated triblock copolymer + photo-initiator	Millimetre-scale lattices	Compressive strength corresponding to trabecular bone Excellent bioactivity	Bone implants	Z. Wang et al., [2022]	[57]
Direct ink writing combined with UV curing + thermal crosslinking + pyrolysis	Polymer ceramic precursor + block copolymers	Ceramic scaffolds with hierarchical porosity	High resistance to flame;pliable structures after printing and curing	Flame-resistant structures;high temperature insulation	Bowen et al., [2022]	[58]
Direct ink writing + thermal crosslinking	Colloidal suspension of Fe_3O_4 NPs, surface treated with oleic acid, dispersed in toluene and crosslinked post-printing	Needle-like structures, diameter exceeding 100 μm, length in the mm scale	Bending properties governed by structural defects (pores), not by ligand forces	Multifunctional devices	Doménech et al., [2020]	[59]
Direct ink writing (direct-write colloidal assembly)	Colloidal suspensions of monodispersed polystyrene nanoparticles (also, silica nanoparticles and gold nanocrystals)	Needle-like structures, diameter exceeding 100 μm, length in the mm scale	Structural colours through Bragg reflection	Optical devices, new materials in photonics and electronics	Tan et al., [2018]	[60]
Piezoelectric drop-on-demand	Colloidal suspension of gold nanoparticles in toluene	Needle-like structures, diameter exceeding 100 μm, length in the mm scale	Clean bottom-up growth of micro-wires with tunable diameter and pocketed structure	New connectors for micro-electronic devices	Kullmann et al., [2012]	[61]
Material extrusion (syringe) bioprinting	Gelatin methacryloyl (gelMA) droplets dynamically bridged by charged silicate nanoplatelets	Grids;helicoid parts	Shear-yielding behaviour	In situ tissue engineering, regeneration, and modeling	Ataie et al., [2022]	[62]
Material extrusion (direct writing)	Laponite (nanoclay)-hydrogel composite suspensions	Millimetre-scale geometries	Direct writing of soft hydrogels not requiring supporting bath	Enabling of bioprinting of soft hydrogel structures	Jin et al., [2017]	[65]
Selective laser melting	Graphene oxide electrostatically attracted onto AlSi10Mg spherical microparticles through hetero-agglomeration process	Millimetre-scale cylinders	Fine grains with Al_2O_3 nanoparticles aggregated at the grain boundaries Graphene oxide absent in finished parts, as dissolved and resolidified in surface carbon layer	Extending the capability of metal AM (easing the laser processing of aluminium alloys)	Dong et al., [2020]	[66]
Metal AM (prospective)	$Ti_3C_2T_x$ MXene electrostatically adsorbed onto aluminium micro-flakes	Compressed billets, with and without annealing	Increased Vickers hardness of compressed billets, depending on MXene concentration and exfoliation	Continuous composite network for multi-functional structural and/or conductive purposes	Wyatt and Anasori [2022]	[67]
Laser-based powder bed fusion	$Ti_3C_2T_x$ MXene electrostatically attracted onto aluminium spherical microparticles	Millimetre-scale cuboids	Improved printability due to laser absorptivity of MXene	Extending the capability of metal AM	W. Zhou et al., [2022]	[68]

(*continued on next page*)

Table 2 (*continued*)

Technique	Material	Printed objects	Outcomes	Applications	Reference	No.
Stereolithography + wet chemical bath deposition of manganese oxide + pyrolysis	Pyrolysable commercial resin, pyrolysed + manganese oxide coating	Supercapacitors having complicated lattice architecture	Nanostructures and distribution density tailorable through precursor concentration	Hybrid supercapacitors	Rezaei et al., [2022]	[70]
Drop-on-demand on cold sink (−25°) + soaking in liquid nitrogen + freeze drying + thermal annealing/reduction	Water-based ink of graphene oxide (structural material) Neat water (support material)	Macroscale prototypes	Exceptional mechanical and functional properties	Scalable fabrication of advanced multifunctional graphene monoliths	Zhang et al., [2016]	[147]
Selective laser sintering	Polystyrene and polystyrene/SiO_2 composite supraparticles from spray-drying of primary colloidal nanoparticles	Millimetre-scale single-layer squares	Even distribution of nanosilica	Extending the capability of SLS through new printable materials	Canziani et al., [2020]	[151]
Selective laser sintering	Polymethyl methacrylate and polymethyl methacrylate/SiO_2 composite supraparticles from spray-drying of primary colloidal nanoparticles	Millimetre-scale two-layered squares	Even distribution of nanosilica	Extending the capability of SLS through new printable materials	Canziani et al., [2021]	[152]
Selective laser sintering	Poly(L-lactide), poly(L-lactide)/SiO_2, and poly(L-lactide)/hydroxyapatite composite supraparticles from spray-drying of primary colloidal nanoparticles	Millimetre-scale squares	Bioactive and biocompatible printed samples	Extending the capability of SLS through new printable materials	Canziani et al., [2022]	[153]
Fused filament fabrication	Self-assembled lignin nanospheres used as filler in PLA	Macroscale testing specimens	Around 0.5% of ligning is enough for reinforcing PLA	Sustainable materials for fused filament fabrication	Long et al., [2022]	[155]
Bioprinting	Self-assembled peptide to provide alginate-microcrystalline cellulose inks with biological features	Millimetre-scale lattices	Cells were more likely to promote adhesive interactions with the material rather than with the other cells	Tissue engineering	Hernández-Sosa et al., [2022]	[156]
Bioprinting + thermal annealing	Self-assembled granulate hydrogel obtained from layer-by-layer graphene oxide-coated agarose microbeads	Millimetre-scale lattices	Annealing above the melting temperature of agarose (60 °C) changes graphene oxide to reduced graphene oxide and promotes a structural reorganisation of agarose to a monolithic hydrogel with hollow micropores	Soft and electrically conductive biomedical devices (biosensors, scaffolds)	Park et al., [2022]	[157]
Bioprinting + layer-by-layer coating deposition	HDPE + multi-layer coating with polydopamine, ε-polylysine, and fibrin	Millimetre-scale lattices Ear prototypes	Self-assembled coating providing bio-activity and antibacterial properties	Scaffolds for auricle reconstruction	Yin et al., [2022]	[158]

arrangement of ordered structures may initially require energy (for example, in the form of stirring). However, once the equilibrium is reached, the system becomes stable and does not dissipate energy anymore. Conversely, in dynamic self-assembly the interactions that are responsible for the arrangement of matter only proceed if the system is dissipating energy. This is the case with biological cells, for example, as opposed to molecular crystals that are the result of static self-assembly [9]. As such, most occurrences of SAMAM in the literature harness the static self-assembly of molecules and particles, whilst the study of dynamic self-assembly is still in its infancy. However, the integration of biologically-inspired organisation of matter in AM closely resonates with the basic concepts of bionics [148], and this opens up new exciting opportunities to translate designs and solutions inspired by nature to advanced technology systems. Historically, a discrepancy has been recognised between the "fabrication" of artificial devices, whereby engineers and developers start from conceiving the part's design and then select the material that best corresponds to the realisation of that design, and the "growth" of biological constructs, whereby nature grows both the material and the whole organism at the same time through self-assembly mechanisms that are directed by the genetic code like an algorithm. Incorporating AM and self-assembly will hopefully contribute to closing the gap between the "fabrication" and "growth" paradigms [149].

As seen before, the majority of the literature explores the utility of self-assembly to advance AM through the development of new printable materials, multi-scale hierarchical structures and embedded functionality. The limited availability of printable materials is currently perceived as a major obstacle to the industrial uptake of AM [150]. A clear demonstration is provided by selective laser sintering (SLS) that, in spite of being a relatively popular polymer-based AM technique, mainly works with polyamide 12 and polyamide 11 powders, whilst a few other polymers like polyethylene (PE), polypropylene (PP), and polyether ether ketone (PEEK) remain niche products. Self-assembled supraparticles produced by spray drying of colloidal suspensions of primary NPs have the potential to widen the palette of printable materials for SLS, including new polymers and composite systems [151–153]. The advent of anisotropic NPs that feature exotic shapes (for example, cubes, icosahedra, triangles, tetrahedra, tripods, stars, just to name a few) or possess areas with different surface functionality ("interaction patchiness", as demonstrated in Fig. 7: for example, surface regions having distinct charges, or having different chemical affinity, like hydrophobic and hydrophilic segments,) can further expand the range of attainable structures with respect to conventional isotropic spherical NPs [154].

Self-assembly can also serve to produce novel fillers that endow AM parts with superior mechanical performance (for example, the self-assembled lignin nanospheres developed by Long et al. [155]) and with ancillary properties (for example, the self-assembled peptide that promotes cell adhesion to bioprinted scaffolds in the contribution by Hernández-Sosa et al. [156]). Traditional trade-offs in materials properties can be surpassed. For example, as shown in Fig. 8 most electrically conductive fillers (including metals and carbonaceous particles) are extremely stiff, and their incorporation unavoidably increases the Young's modulus of the polymer matrix. However, thanks to the

Table 3
Examples of experimental research in SAMAM through 3D printing-enabled mechanisms (listed according to the in-text reference number as shown in the last column).

Technique	Material	Printed objects	Outcomes	Applications	Reference	No.
Inkjet printing (prospective)	Water suspensions of single-walled carbon-nanotubes	Sessile droplets	Study of evaporation dynamics	Advancement of 3D printed electronics	Goh et al., [2019]	[71]
Inkjet printing	Graphene/terpineol dispersion with ethanol (rheology)	Thin films and sub-millimetre electronic devices	Achievement of printed graphene (not graphene oxide)	Enabling the inkjet printing of graphene for organic and printed electronics	Li et al., [2013]	[72]
Inkjet printing	Water suspension of multi-walled carbon-nanotubes	Millimetre-scale tracks with high lateral resolution	Coffee ring-enabled printing of tracks with width of 5–15 μm	Micrometre-wide conductive electrodes	Dinh et al., [2016]	[73]
Inkjet printing	Water suspension of single-walled carbon-nanotubes	Millimetre-scale films	Control of the filler alignment through ink concentration	Large-area electronics and sensors	Beyer and Walus [2012]	[74]
Fused filament fabrication	ABS-matrix composites with graphene or carbon nanotubes oriented after flow forces	Macroscale testing specimens	Anisotropy in mechanical and functional properties coming from flow-induced orientation	Electronic devices	Dorigato et al., [2017]	[77]
Fused filament fabrication + crosslinking via thermal annealing	Aromatic thermotropic (liquid crystal) polyesters	Layers (laminae); macroscale prototypes	Rasters receiving core-shell structure due to flow orientation and subsequent cooling Stiffness and strength increasing with skin thickness	Increasing mechanical strength without fibres, thus retaining shaping freedom	Gantenbein et al., [2018]	[78]
Flow-induced structural ordering in material extrusion AM + selective biomimetic crystallisation of calcium phosphate	Di-acrylate modified, amphiphilic triblock copolymers (BCPs) self-assembled into nano micellar fibrils (NMFs) with biomimetic crystallisation of calcium phosphate	Bone fixture	Compressive response controlled by intrinsic features (molecular weight of the starting BCPs and alignment of the NMFs at the nanoscale) and by extrinsic features (micro- and macroscopic architecture governed by CAD file)	Bone implants	Rajasekharan et al., [2018]	[81]
Digital light processing with linear oscillator	Acrylate based photocurable polymer + surface-treated alumina nanofibres	Macroscale (tensile) testing specimens	Improved tensile properties only after surface treatment to the filler	Achievement of conceptually new composite materials	Yunus et al., [2016]	[83]
Vat photopolymerisation combined with journal bearing laminar flow set-up	Ink drop (a pregel drop, a suspension of fluorescent particles, nanoparticles, or cells) injected into a viscous polymer resin	Millimetre-scale discs	Chaotic printing, but predictable length of the stretched drop	Systems with high surface area per unit volume (densely packed) for catalytic surfaces and tissue-like structures in biomedical and electronics applications	Trujillo-De Santiago et al., [2018]	[84]
Laser-based powder bed fusion	Copper: dislocation manipulation	Testing specimens	Self-arrangement of dislocations breaking conventional strength-ductility trade off	Manipulation of the mechanical behaviour of metal parts by PBF	Li et al., [2021]	[88]
Selective laser melting	Eutectic high entropy alloy	Testing specimens	Improved mechanical properties through refined lamellar eutectic structure	Improved materials for SLM	F. Yang et al., [2022]	[133]

alignment of elongated conductive fillers, or thanks to the spontaneous arrangement of conductive fillers to create a segregated network, the percolation threshold in soft polymer-matrix composites can be attained with a relatively low filler loading, thus sidestepping any disadvantageous compromise between conductivity and flexibility in 3D printed wearable sensors and soft tissue scaffolds (as demonstrated, for example, by Park et al. [157]). Many 4D printed systems owe their actuation ability and stimuli responsiveness to the self-ordered arrangement of matter [4,32,96,99,100]. Self-assembled coatings may impart new functionality to AM parts after printing [70,158].

As such, self-assembly appears to be a precious aid to enlarging the capability of AM. However, in principle also the opposite may apply, and AM may become an important aid to enabling the self-assembly of multiscale structures. For example, Zhou et al. [159] and Yang et al. [160] 3D printed complicated lattice structures having hollow struts by DLP and used them as templates for the self-assembly of various functional NPs. MXene or graphene oxide inks were injected into the hollow struts, and then converted to self-assembled self-standing hydrogels. Finally, the resin templates were removed through selective chemical etching to reveal the additive-free NP-based lattices. Whilst the efficient self-assembly of NPs can be difficult in long-range ordered structures, the 3D printed hollow frames offer a confined space, which is ideal for the spontaneous arrangement of matter. In this way, the lattice architecture can be controlled at the meso- to macro-scale through the AM design, and at the nano- to micro-scale through the self-assembly process [159,160]. Owing to the difficulty of formulating printable inks, this AM-enabled self-assembly of graphene-based materials appears particularly advantageous [161]. As proved by Zhou et al. [159], the polymer template-mediated procedure can also be extended to other NP inks, including various ceramics such as titania and alumina. This may thus be the starting point for a new area of research, where AM meets self-assembly (AMMSA).

Finally, it should also be mentioned that, sometimes, accurate investigation is required to prevent the self-assembly of matter, as this may be detrimental to printability. Collagen type 1, for example, has been identified as the most abundant collagen in the human cornea. However, 3D printing a bioengineered cornea starting from a collagen-based bio-ink can be extremely difficult, due to the natural tendency of collagen type 1 to self-assemble/self-gel in vitro at physiological pH. The identification of buffer solutions impairing the self-assembly is thus crucial for extending the applicability of collagen type 1-based bio-inks in corneal printing [162]. This example suggests that additional knowledge is still necessary to understand when self-assembly can assist AM, when AM can assist self-assembly, and when AM and self-assembly should not

Table 4
Examples of experimental research in SAMAM through field-assisted mechanisms (listed according to the in-text reference number as shown in the last column).

Technique	Material	Printed objects	Outcomes	Applications	Reference	No.
Magnetic field-assisted direct ink writing + mask-assisted photocuring	Alumina platelets decorated with iron-oxide nanoparticles in photocurable resin + fumed silica to adjust rheology for DIW	Macroscale prototypes	Composition and alignment controlled independently Hygromorphism	New dimensionality in 3D printing design space	Kokkinis et al., [2015]	[96]
Magnetic field-assisted direct light processing	Alumina platelets decorated with iron-oxide nanoparticles in photocurable resin	Macroscale prototypes	Composition and alignment controlled independently Crack steering	Bioinspired structures with increased mechanical resistance	Martin et al., [2015]	[98]
Magnetic field-assisted stereolithography	Ferromagnetic γ-Fe_2O_3 short fibres in photocurable resin	Millimetre-scale specimens	4D printed structures actuated remotely by magnetic field	4D printing	Nakamoto and Marukado [2016]	[99]
Magnetic field-assisted direct ink writing	Neodymium alloy as the active filler in a silicone rubber matrix + fumed silica to adjust rheology for DIW	Macroscale prototypes	Exceptional morphing ability enable by soft matrix and programmed through finite element simulations	Next generation of smart actuators	Kim et al., [2018]	[100]
Electric field-assisted vat photopolymerisation	Aluminium micro-particles in acrylated photopolymer	Macroscale prototypes	Build-up of continuous fibre-like reinforcement through self-assembled chains of discrete particles	Devices with tunable properties Military applications	Holmes and Riddick [2014]	[108]
Electric field-assisted fused filament fabrication + corona poling	Polyvinylidene fluoride (PVDF)	Macroscale (thin) testing specimens	<beta> phase depending on printing parameters	New piezoelectric sensors and devices	Porter et al., [2017]	[110]
Acoustic-assisted bioprinting (syringe material extrusion)	Mixture of C2C12 cells or human umbilical vein endothelial cells (HUVECs)-embedded gelatin methacryloyl (GelMA)	Millimetre-scale specimens	Efficient accumulation of cells at the middle of the printed construct and significant cell elongation in the printing direction	Spatially controlled bioprinting to simulate complex and highly organized native tissues	Sriphutkiat et al., [2019]	[113]
Acoustic-assisted custom-made stereolithography	Chopped glass fibres in low viscosity photocurable resin	Millimetre-scale geometries	Orthogonally oriented fibres in subsequent layers, but only demonstrated with few layers	Achievement of conceptually new composite materials	Llewellyn et al., [2016]	[119]
Acoustic field-assisted direct ink writing	Various composite materials (review)	Millimetre-scale geometries	Combination of shear-induced alignment and acoustic focusing	Achievement of conceptually new composite materials Decreasing percolation threshold	Johnson et al., [2021]	[121]
Acoustic-assisted digital light processing with rotating base platform	Yttria particles in photocurable resin arranged in discontinuous interpenetrating-phase composite	Millimetre-scale cuboids	Increased energy absorption under compressive load due to progressive localized failure	Achievement of conceptually new composite materials	Li et al., [2022]	[122]
Magnetic field-assisted directed energy deposition	Inconel IN718	Millimetre-scale cuboids	Dendrite spacing increased and epitaxial growth governed through altered Marangoni convection	Extending the capability of metal AM	Du et al., [2020]	[127]
Magnetic field-assisted selective laser melting	Commercially pure titanium (CP–Ti)	Millimetre-scale cuboids	Higher tensile strength and ductility owing to microstructure refining and homogenising, and elimination of texture	Extending the capability of metal AM	Kang et al., [2017]	[128]
Acoustic field-assisted directed energy deposition	Ti–6Al–4V	Millimetre-scale cuboids	Improved yield and tensile strength owing to transition from columnar grains to fine equiaxed grains	Extending the capability of metal AM	Todaro et al., [2020]	[129]
Magnetic field-assisted selective laser melting	Stainless steel SS316L	Millimetre-scale cuboids	Higher ductility owing to inhibition of epitaxial growth and texture	Extending the capability of metal AM	H. Zhou et al., [2022]	[130]
Electric field-assisted mask-image-projection-based stereolithography with rotating electric field	Epoxy di-acrylated resin + surface-treated multi-wall carbon nanotubes	Millimetre-scale Menger sponges with Bouligand structure. Centimetre-scale meniscus model	Smaller rotation angle leading to greater energy dissipation and impact resistance	Bioinspired structures with increased mechanical resistance Biomedical application	Yang et al., [2017]	[144]

interact at all.

5. Challenges and outlook

Fig. 9 provides a graphical summary of the main opportunities and limitations associated with SAMAM.

As already discussed in Section 5, one of the main advantages afforded by SAMAM is the development of new printable materials. Although AM is already an enabling technology of the Industry 4.0 revolution, many industries, such as aerospace and aviation, biomedicine, and defence are craving for the ability to 3D print new functional materials with customisable advanced features, such as biocompatibility and bioactivity, radiation shielding, thermal and electrical conductivity, high strength, self-sensing and self-repair, stimuli responsiveness, flexibility and softness [21]. SAMAM can certainly contribute to expanding the palette of printable materials and thus facilitate the advancement of AM in industrial settings.

Additionally, conventional trade-offs in materials properties can be worked out through SAMAM. For example, in MEX the amount of filler required to establish a conductive percolation pathway can be minimised

Table 5
Examples of experimental research in AMMSA, wherein AM is leveraged to assist in self-assembly of matter (listed according to the in-text reference number as shown in the last column).

Technique	Material	Printed objects	Outcomes	Applications	Reference	No.
Digital light processing	Injection of graphene oxide ink into hollow lattice structure, self-assembly through hydrothermal reduction or through freeze casting, and chemical etching of polymer template	Millimetre-scale lattices	Tunable mechanical properties (compression) High adsorption capacity for chloroform	Scalable fabrication of advanced multifunctional graphene monoliths Approach applicable to other materials	J. Zhou et al., [2022]	[159]
Digital light processing	Injection of $Ti_3C_2T_x$ MXene ink into hollow lattice structure, self-assembly through cation-induced gelation process, and chemical etching of polymer template	Millimetre-scale lattices	High areal capacitance and energy density	Electrodes in microsupercapacitors	C. Yang et al., [2022]	[160]
Mask-image-projection-based stereolithography	Injection of GO/ethylenediamine (EDA) ink into the hollow polymer template, hydrothermal assembly in autoclave, freeze-drying, thermal etching of polymer template	Millimetre-scale lattices	Exceptional mechanical and functional properties	Scalable fabrication of advanced multifunctional graphene monoliths	Zhang et al., [2018]	[161]

through the self-assembly of matter, thus preserving the flexibility and softness of the polymer matrix [157].

Although less obvious, the design of new functional materials and more efficient devices may offer important advantages in terms of eco-sustainability [163]. A significant example comes from electrically conductive materials. According to numbers cited by Baker et al. [164], conventional technologies for producing metal-based printed circuit boards (PCBs) are responsible for substantial amounts of waste, to the point that the etching step alone is deemed responsible for 1×10^{12} L of chemical waste per year worldwide. As recently argued by Pejak Simunec and Sola [109], polymer-based composite materials and blends with self-assembled microstructure through shear-induced alignment or segregated networks have the potential to replace conventional metal-based materials in the fabrication of electronic devices, with substantial benefits for the environment.

Another key strength of SAMAM is the ability to manipulate structural features across multiple length scales as demonstrated, for instance, by the hierarchical lattices in the research conducted by Z. Wang et al. [57]. AM technologies are currently unable to target nanoscale properties in macroscale objects and this represents a serious impediment to the uptake of AM in many industrial sectors such as the production of membranes for water treatment and filtration [165–167].

SAMAM can also result in process intensification. Owing to the bottom-up approach, new or increased functionality can be achieved upon printing. As proved by Li et al. [88], for example, in laser-based PBF the self-organisation of dislocations into an inter-pinned configuration produces self-strengthened parts in the as-built state, without any additional heat treatment. This eliminates the need for lengthy post-processing steps, which are incompatible with the industrial expectation for shorter lead times through the adoption of AM.

Although the self-assembly of matter has occasionally been reported to curb the printability of certain materials [162], SAMAM *per se* does not have true disadvantages, as it is meant to be the intentional adoption of self-assembly to aid in AM. Rather, SAMAM still has some limitations. As previously observed, research has mainly been addressed to polymers, whilst metals are still relatively rare in the literature and additional efforts are certainly needed to bridge this gap. It is worth noting that even less attention has been paid to ceramics and glasses. Broadly speaking, ceramics and glasses represent a challenge because their exceptional thermal stability is an obstacle to inter-layer bonding and consolidation in AM. Moreover, they are often brittle and particularly sensitive to thermal-stress induced cracking [168]. In future, it would be interesting to explore the effectiveness of SAMAM to facilitate AM of ceramics and glasses.

Although encouraging results have recently been published in this regard (for example, in the contribution by Zhang et al. [147]), at present it is not clear yet if SAMAM can actually be instrumental in mitigating the weak interlayer adhesion often observed in AM constructs. In particular, most approaches to field-assisted SAMAM control the microstructure within individual layers, thus minimally contributing to the achievement of a continuous distribution of fillers across the print layers.

Whilst knowledge progresses, it would be useful to adopt a standard nomenclature and to outline a general roadmap to SAMAM. To this aim, as a starting point, Tables 2–4 classify the literature discussed in the present review according to the proposed categories of "SAMAM through local interactions", "3D printing-enabled SAMAM", and "Field-assisted SAMAM", respectively. For the reader's convenience, the contributions are listed according to their in-text reference number as shown in the last column. For each research article, Tables 2–4 summarise experimental conditions, main outcomes and intended applications. For the sake of completeness, Table 5 records the same information for AMMSA-related works (i.e, for contributions that harness AM as an aid to self-assembly of matter). These tables will hopefully provide a reference for developers and scientists engaged in SAMAM and a general framework for future research.

6. Conclusions

Conventional additive manufacturing methods are ideal for customising a part's geometry at the macroscale, typically in the sub-millimetre to centimetre range. However, apart from few exceptions, they do not allow the material's composition and structure to be tuned in the nanometre to micrometre range. Since the material's behaviour is dictated by its structure, the lack of control of nano- and micro-scale features undermines the achievement of the desired functional and mechanical properties. The combination of self-assembly and additive manufacturing ("self-assembly meets additive manufacturing", SAMAM) is a promising avenue of overcoming present-day hurdles to enable the construction of "spontaneously nanostructured" parts with customised features over a variety of length scales. SAMAM can be accomplished through numerous methods, which can be classified in three main categories. Self-assembly can occur locally, owing to attractive or repulsive forces between molecules or nanoparticles, such as electrostatic forces or chemical interactions governed by functional groups. Otherwise, self-assembly can be triggered by forces that spontaneously generate upon printing, such as the flow-induced shear stresses in material extrusion technologies. Finally, molecules and fillers can be oriented and patterned through externally applied forces in field-assisted AM (directed assembly). Besides enabling the achievement of hierarchical structures, SAMAM can be leveraged to develop new printable materials and overcome conventional trade-offs in materials properties. Given the limited range of printable feedstocks currently available in the marketplace, the design of new materials is crucial for the uptake of additive manufacturing in numerous industries, from the biomedical field to aviation and aerospace, from

defence to electronics. Assisted by SAMAM, more efficient products can be obtained in a single step upon printing without additional post-processing. This is expected to reduce the lead time (process intensification) and the environmental footprint of additive manufacturing. However, in order to take full advantage of the opportunities afforded by SAMAM, additional research is needed in metal- and ceramic-based systems. Special attention should be paid to new avenues of mitigating the weak inter-layer adhesion that is often blamed on the layer-by-layer build-up mechanisms in additive manufacturing.

Declaration of competing interest

The authors declare that they have no known competing financial interests or personal relationships that could have appeared to influence the work reported in this paper.

Acknowledgments

AS is supported by the Commonwealth Scientific and Industrial Research Organisation (CSIRO) Research Office, Australia, through the "Science Leader in Active Materials" platform.

References

[1] J.R. Greer, J. Park, Additive manufacturing of nano- and microarchitected materials, Nano Lett. 18 (2018) 2187–2188, https://doi.org/10.1021/acs.nanolett.8b00724.
[2] V. Harinarayana, Y.C. Shin, Two-photon lithography for three-dimensional fabrication in micro/nanoscale regime: a comprehensive review, Opt Laser. Technol. 142 (2021), https://doi.org/10.1016/j.optlastec.2021.107180 eid:107180.
[3] Q. Ge, Z. Li, Z. Wang, K. Kowsari, W. Zhang, X. He, J. Zhou, N.X. Fang, Projection micro stereolithography based 3D printing and its applications, Inter. J. Extreme Manufac. 2 (2020), https://doi.org/10.1088/2631-7990/ab8d9a eid:022004.
[4] B. Elder, R. Neupane, E. Tokita, U. Ghosh, S. Hales, Y.L. Kong, Electrically conductive nanocomposites for fused deposition modelling, Adv. Mater. 32 (2020), https://doi.org/10.1002/adma.201907142 eid:1907142.
[5] M. Mao, J. He, X. Li, B. Zhang, Q. Lei, Y. Liu, D. Li, The emerging frontiers and applications of high-resolution 3D printing, Micromachines 8 (4) (2017), https://doi.org/10.3390/mi8040113 eid:113.
[6] J. Yang, B. Zhou, D. Han, N. Cui, B. Li, J. Shen, Z. Zhang, A. Du, High-precision three-dimensional printing in a flexible, low-cost and versatile way: a review, ES Mate. Manufac. 15 (2021) 1–13, https://doi.org/10.30919/esmm5f526.
[7] G. Yang, X. Huang, C. Jia, Direct writing of 3D micro/nanostructures based on nanoscale strong electric field of electron beam, Adv. Eng. Mater. (2022), https://doi.org/10.1002/adem.202200822 eid:2200822 early view.
[8] N.B. Crane, J. Tuckerman, G.N. Nielson, Self-assembly in additive manufacturing: opportunities and obstacles, Rapid Prototyp. J. 17 (3) (2011) 211–217, https://doi.org/10.1108/13552541111124798.
[9] G.M. Whitesides, B. Grzybowski, Self-assembly at all scales, Science 295 (2002) 2418–2421, https://doi.org/10.1126/science.1070821.
[10] S. Wintzheimer, T. Granath, M. Oppmann, T. Kister, T. Thai, T. Kraus, N. Vogel, K. Mandel, Supraparticles: functionality from uniform structural motifs, ACS Nano 12 (2018) 5093–5120, https://doi.org/10.1021/acsnano.8b00873.
[11] P.Q. Nguyen, N.-M.D. Courchesne, A. Duraj-Thatte, P. Praveschotinunt, N.S. Joshi, Engineered living materials: prospects and challenges for using biological systems to direct the assembly of smart materials, Adv. Mater. 30 (2018), https://doi.org/10.1002/adma.201704847 eid:1704847.
[12] H.M. Jonkers, Bacteria-based self-healing concrete, Heron 56 (2011) 1–12 [Online]. Available: http://heronjournal.nl/56-12/1.pdf.
[13] Y. Ze, R. Wang, H. Deng, Z. Zhou, X. Chen, L. Huang, Y. Yao, Three-dimensional bioprinting: a cutting-edge tool for designing and fabricating engineered living materials, Biomater. Advan. (2022), https://doi.org/10.1016/j.bioadv.2022.213053 eid:213053.
[14] K.S. Hald, P. Coslugeanu, The preliminary supply chain lessons of the COVID-19 disruption - what is the role of digital technologies? Opera. Manag. Res. 15 (2022) 282–297, https://doi.org/10.1007/s12063-021-00207-x.
[15] H.A. Colorado, D.E. Mendoza, H.-T. Lin, E. Gutierrez-Velasquez, Additive manufacturing against the covid-19 pandemic: a technological model for the adaptability and networking, J. Mater. Res. Technol. 16 (2022) 1150–1164, https://doi.org/10.1016/j.jmrt.2021.12.044.
[16] Y.Y.C. Choong, H.W. Tan, D.C. Patel, W.T.N. Choong, C.-H. Chen, H.Y. Low, M.J. Tan, C.D. Patel, C.K. Chua, The global rise of 3D printing during the COVID-19 pandemic, Nat. Rev. Mater. 5 (2020) 637–639, https://doi.org/10.1038/s41578-020-00234-3.
[17] M.S. Tareq, T. Rahman, M. Hossain, P. Dorrington, Additive manufacturing and the COVID-19 challenges: an in-depth study, J. Manuf. Syst. 60 (2021) 787–798, https://doi.org/10.1016/j.jmsy.2020.12.021.
[18] N. Li, S. Huang, G. Zhang, R. Qin, W. Liu, H. Xiong, G. Shi, J. Blackburn, Progress in additive manufacturing on new materials: a review, J. Mater. Sci. Technol. 35 (2019) 242–269, https://doi.org/10.1016/j.jmst.2018.09.002.
[19] T.D. Ngo, A. Kashani, G. Imbalzano, K.T. Nguyen, D. Hui, Additive manufacturing (3D printing): a review of materials, methods, applications and challenges, Compos. B Eng. 143 (2018) 172–196, https://doi.org/10.1016/j.compositesb.2018.02.012.
[20] A. Sola, A. Trinchi, 3 - the need for fused deposition modeling of composite materials, in: A. Sola, A. Trinchi (Eds.), Fused Deposition Modeling of Composite Materials, 1st ed., U.K.: Elsevier - Woodhead Publishing Series in Composites Science and Engineering, Cambridge, MA, U.S.A. – Kidlington, 2022, pp. 39–88, https://doi.org/10.1016/B978-0-323-98823-0.00004-4.
[21] S.A. Tofail, E.P. Koumoulos, A. Bandyopadhyay, S. Bose, L. O'Donoghue, C. Charitidis, Additive manufacturing: Scientific and technological challenges, market uptake and opportunities, Mater. Today 21 (1) (2018) 22–37, https://doi.org/10.1016/j.mattod.2017.07.001.
[22] Z. Fan, X. Yan, Z. Fu, B. Niu, J. Chen, Y. Hu, C. Chang, J. Yi, In situ formation of D022-Al3Ti during selective laser melting of nano-TiC/AlSi10Mg alloy prepared by electrostatic self-assembly, Vacuum 188 (2021), https://doi.org/10.1016/j.vacuum.2021.110179 eid:110179.
[23] C.Y. Yap, C.K. Chua, Z.L. Dong, Z.H. Liu, D.Q. Zhang, L.E. Loh, S.L. Sing, Review of selective laser melting: materials and applications, Appl. Phys. Rev. 2 (2015), https://doi.org/10.1063/1.4935926 eid:041101.
[24] J.H. Martin, B.D. Yahata, J.M. Hundley, J.A. Mayer, T.A. Schaedler, T.M. Pollock, 3D printing of high-strength aluminium alloys, Nature 549 (2017) 365–369, https://doi.org/10.1038/nature23894.
[25] W. Zhao, Y. Yan, X. Chen, T. Wang, Combining printing and nanoparticle assembly: methodology and application of nanoparticle patterning, Innovation (2022), https://doi.org/10.1016/j.xinn.2022.100253 eid:100253.
[26] H.J. Park, S. Cho, M. Kim, Y.S. Jung, Carboxylic acid-functionalized, graphitic layer-coated three-dimensional SERS substrate for label-free analysis of Alzheimer's disease biomarkers, Nano Lett. 20 (2020) 2576–2584, https://doi.org/10.1021/acs.nanolett.0c00048.
[27] S. Yim, S. Jeon, J.M. Kim, K.M. Baek, G.H. Lee, H. Kim, J. Shin, Y.S. Jung, Transferrable plasmonic Au thin film containing sub-20 nm nanohole array constructed via high-resolution polymer self-assembly and nanotransfer printing, ACS Appl. Mater. Interfaces 10 (3) (2018) 2216–2223, https://doi.org/10.1021/acsami.7b16401.
[28] L. Siebert, N. Wolff, N. Ababii, M.-I. Terasa, O. Lupan, A. Vahl, V. Duppel, H. Qiu, M. Tienken, M. Mirabelli, V. Sontea, F. Faupel, L. Kienle, R. Adelung, Facile fabrication of semiconducting oxide nanostructures by direct ink writing of readily available metal microparticles and their application as low power acetone gas sensors, Nano Energy 70 (2020), https://doi.org/10.1016/j.nanoen.2019.104420 eid:104420.
[29] ISO/ASTM 52900:2021, additive manufacturing – general principles – fundamentals and vocabulary, ISO, Tech.Comm. ISO/TC 261 Additive Manufac.; ASTM (2021), https://doi.org/10.1520/F3177-21. Subcommittee: F42.91 on Terminology, Standard.
[30] M. Roy, P. Tran, T. Dickens, A. Schrand, Composite reinforcement architectures: a review of field-assisted additive manufacturing for polymers, J. Compos. Sci 4 (2020), https://doi.org/10.3390/jcs4010001 eid:1.
[31] J. Li, Q. Ye, A. Cassell, H.T. Ng, R. Stevens, J. Han, M. Meyyappan, Bottom-up approach for carbon nanotube interconnects, Appl. Phys. Lett. 82 (2003) 2491–2493, https://doi.org/10.1063/1.1566791.
[32] W. Xu, S. Jambhulkar, D. Ravichandran, Y. Zhu, M. Kakarla, Q. Nian, B. Azeredo, X. Chen, K. Jin, B. Vernon, D.G. Lott, J.L. Cornella, O. Shefi, G. Miquelard-Garnier, Y. Yang, K. Song, 3D printing-enabled nanoparticle alignment: a review of mechanisms and applications, Small 17 (2021), https://doi.org/10.1002/smll.202100817 eid:2100817.
[33] Y. Min, M. Akbulut, K. Kristiansen, Y. Golan, J. Israelachvili, The role of interparticle and external forces in nanoparticle assembly, Nat. Mater. 7 (2008) 527–538, https://doi.org/10.1038/nmat2206.
[34] A. Stannard, Dewetting-mediated pattern formation in nanoparticle assemblies, J. Phys. Condens. Matter 23 (2011), https://doi.org/10.1088/0953-8984/23/8/083001 eid:083001.
[35] F.C. Godoi, S. Prakash, B.R. Bhandari, 3D printing technologies applied for food design: status and prospects, J. Food Eng. 179 (2016) 44–54, https://doi.org/10.1016/j.jfoodeng.2016.01.025.
[36] H. Wang, L. Hu, L. Peng, J. Du, M. Lan, Y. Cheng, L. Ma, Y. Zhang, Dual encapsulation of β-carotene by β-cyclodextrin and chitosan for 3D printing application, Food Chem. 378 (2022), https://doi.org/10.1016/j.foodchem.2022.132088 eid:132088.
[37] H. Wang, Z. Ouyang, L. Hu, Y. Cheng, J. Zhu, L. Ma, Y. Zhang, Self-assembly of gelatin and phycocyanin for stabilizing thixotropic emulsions and its effect on 3D printing, Food Chem. 397 (2022), https://doi.org/10.1016/j.foodchem.2022.133725 eid:133725.
[38] E. Pulatsu, J.-W. Su, J. Lin, M. Lin, Utilization of ethyl cellulose in the osmotically-driven and anisotropically-actuated 4D printing concept of edible food composites, Carbohydrate Polymer Technologies and Carbohydrate Polymer Tech. Appl. 3 (2022), https://doi.org/10.1016/j.carpta.2022.100183 eid:100183.
[39] A. Ahmed, S. Arya, V. Gupta, H. Furukawa, A. Khosla, 4D printing: fundamentals, materials, applications and challenges, Polymer 228 (2021), https://doi.org/10.1016/j.polymer.2021.123926 eid:123926.
[40] X. Kuang, D.J. Roach, J. Wu, C.M. Hamel, Z. Ding, T. Wang, M.L. Dunn, H.J. Qi, Advances in 4D printing: materials and applications, Adv. Funct. Mater. 29 (2019), https://doi.org/10.1002/adfm.201805290 eid:1805290.

[41] S.C. Ligon, R. Liska, J. Stampfl, M. Gurr, R. Mulhaupt, Polymers for 3D printing and customized additive manufacturing, Chem. Rev. 117 (15) (2017) 10,212–10,290, https://doi.org/10.1021/acs.chemrev.7b00074.
[42] A. Mitchell, U. Lafont, M. Hołyńska, C.J.A.M. Semprimoschnig, Additive manufacturing - a review of 4D printing and future applications, Addit. Manuf. 24 (2018) 606–626, https://doi.org/10.1016/j.addma.2018.10.038.
[43] F. Momeni, S.M. Hassani.N, X. Liu, J. Ni, A review of 4D printing, Mater. Des. 122 (2017) 42–79, https://doi.org/10.1016/j.matdes.2017.02.068.
[44] S. Tibbits, 4D printing: multi-material shape change, Architect. Des 84 (2014) 116–121, https://doi.org/10.1002/ad.1710.
[45] A. M. W. Group, Animate Materials – Perspective, Perspective Report, The Royal Society, 6-9 Carlton House Terrace, London, UK, 2021 [Online]. Available: https://www.royalsociety.org/animate-materials.
[46] H. Hamoudi, G.R. Berdiyorov, A. Zekri, Y. Tong, S. Mansour, V.A. Esaulov, K. Youcef-Toumi, Building block 3D printing based on molecular self-assembly monolayer with self-healing properties, Sci. Rep. 12 (1) (2022) 1–9, https://doi.org/10.1038/s41598-022-10875-9.
[47] P. Muller, Glossary of terms used in physical organic chemistry (IUPAC Recommendations 1994), Pure Appl. Chem. 66 (5) (1994) 1077–1184, https://doi.org/10.1351/pac199466051077.
[48] J.-M. Lehn, Supramolecular chemistry, Science 260 (1993) 1762–1763, https://doi.org/10.1126/science.8511582.
[49] J.-M. Lehn, Towards complex matter: supramolecular chemistry and self-organization, Eur. Rev. 17 (2009) 263–280, https://doi.org/10.1017/S1062798709000805.
[50] J.-M. Lehn, Supramolecular chemistry: where from? Where to? Chem. Soc. Rev. 46 (2017) 2378–2379, https://doi.org/10.1039/C7CS00115K.
[51] H. Rupp, W.H. Binder, 3D printing of solvent-free supramolecular polymers, Front. Chem. 9 (2021), https://doi.org/10.3389/fchem.2021.771974 eid:771974.
[52] F. Andriamiseza, D. Bordignon, B. Payré, L. Vaysse, J. Fitremann, 3D printing of biocompatible low molecular weight gels: imbricated structures with sacrificial and persistent N-alkyl-D-galactonamides, J. Colloid Interface Sci. 617 (2022) 156–170, https://doi.org/10.1016/j.jcis.2022.02.076.
[53] X. Bai, Q. Sun, H. Cui, L.P. Guerzoni, S. Wuttke, F. Kiessling, L. De Laporte, T. Lammers, Y. Shi, Controlled covalent self-assembly of a homopolymer for multi-scale materials engineering, Adv. Mater. 34 (39) (2022), https://doi.org/10.1002/adma.202109701 eid:2109701.
[54] H. Honaryar, J.A. LaNasa, E.C. Lloyd, R.J. Hickey, Z. Niroobakhsh, Fabricating robust constructs with internal phase nanostructures via liquid-in-liquid 3D printing, Macromol. Rapid Commun. 42 (2021), https://doi.org/10.1002/marc.202100445 eid:2100444.
[55] M. Demleitner, F. Schönl, J. Angermann, P. Fässler, I. Lamparth, K. Rist, T. Schnur, Y. Catel, S. Rosenfeldt, M. Retsch, H. Ruckdäschel, V. Altstädt, Influence of block copolymer concentration and resin crosslink density on the properties of UV-curable methacrylate resin systems, Macromol. Mater. Eng. 307 (10) (2022), https://doi.org/10.1016/10.1002/mame.202200320 eid:2200320.
[56] G.J.d.A. Soler-Illia, E.L. Crepaldi, D. Grosso, C. Sanchez, Block copolymer-templated mesoporous oxides, Curr. Opin. Colloid Interface Sci. 8 (1) (2003) 109–126, https://doi.org/10.1016/S1359-0294(03)00002-5.
[57] Z. Wang, D. Lin, M. Wang, R. Mao, H. Zhao, X. Huang, S.G. Shen, Seamless route of self-assembly and 3D printing to fabricate hierarchical mesoporous bioactive glass scaffold for customized bone regeneration with enhanced efficacy, Chem. Eng. J. 446 (2022), https://doi.org/10.1016/j.cej.2022.137270 eid:137270.
[58] J. J. Bowen, S. Mooraj, J. A. Goodman, S. Peng, D. P. Street, B. Roman-Manso, E. C. Davidson, K. L. Martin, L. M. Rueschhoff, S. N. Schiffres et al., "Hierarchically porous ceramics via direct writing of preceramic polymer-triblock copolymer inks," Mater. Today, vol 58, pp 71–79, https://doi.org/10.1016/j.mattod.2022.07.002.
[59] B. Domènech, A.T.L. Tan, H. Jelitto, E. Zegarra Berodt, M. Blankenburg, O. Focke, J. Cann, C. Cem Tasan, L. Colombi Ciacchi, M. Müller, K.P. Furlan, A.J. Hart, G.A. Schneider, Strong macroscale supercrystalline structures by 3D printing combined with self-assembly of ceramic functionalized nanoparticles, Adv. Eng. Mater. 22 (2020), https://doi.org/10.1002/adem.202000352 eid:2000352.
[60] A.T.L. Tan, J. Beroz, M. Kolle, A.J. Hart, Direct-write freeform colloidal assembly, Adv. Mater. 30 (2018), https://doi.org/10.1002/adma.201803620 eid:201803620.
[61] C. Kullmann, N.C. Schirmer, M.-T. Lee, S.H. Ko, N. Hotz, C.P. Grigoropoulos, D. Poulikako, 3D micro-structures by piezoelectric inkjet printing of gold nanofluids, J. Micromech. Microeng. 22 (2012), https://doi.org/10.1088/0960-1317/22/5/055022 eid:055022.
[62] Z. Ataie, S. Kheirabadi, J.W. Zhang, A. Kedzierski, C. Petrosky, R. Jiang, C. Vollberg, A. Sheikhi, Nanoengineered granular hydrogel bioinks with preserved interconnected microporosity for extrusion bioprinting, Small 18 (37) (2022), https://doi.org/10.1002/smll.202202390 eid:2202390.
[63] X.-B. Huang, J.-S. Sun, Y. Huang, B.-C. Yan, X.-D. Dong, F. Liu, R. Wang, Laponite: a promising nanomaterial to formulate high-performance water-based drilling fluids, Petrol. Sci. 18 (2021) 579–590, https://doi.org/10.1007/s12182-020-00516-z.
[64] B. Ruzicka, E. Zaccarelli, A fresh look at the laponite phase diagram, Soft Matter 7 (4) (2011) 1268–1286, https://doi.org/10.1039/C0SM00590H.
[65] Y. Jin, C. Liu, W. Chai, A. Compaan, Y. Huang, Self-supporting nanoclay as internal scaffold material for direct printing of soft hydrogel composite structures in air, ACS Appl. Mater. Interfaces 9 (2017) 17,456–17,465, https://doi.org/10.1021/acsami.7b03613.
[66] M. Dong, W. Zhou, K. Kamata, N. Nomura, Microstructure and mechanical property of graphene oxide/AlSi10Mg composites fabricated by laser additive manufacturing, Mater. Character. 170 (2020), https://doi.org/10.1016/j.matchar.2020.110678 eid:110678.
[67] B.C. Wyatt, B. Anasori, Self-assembly and in-situ characterization of Ti3C2Tx in Al: a step toward additive manufacturing of MXene-metal composites, Appl. Mater. Today 27 (2022), https://doi.org/10.1016/j.apmt.2022.101451 eid:101451.
[68] W. Zhou, Z. Zhou, S. Guo, Y. Fan, N. Nomura, Structural evolution mechanism during 3D printing of MXene-reinforced metal matrix composites, Compos. Commun. 29 (2022), https://doi.org/10.1016/j.coco.2021.101034 eid:101034.
[69] Y. Gogotsi, B. Anasori, The rise of MXenes, ACS Nano 13 (2019) 8491–8494, https://doi.org/10.1021/acsnano.9b06394.
[70] B. Rezaei, T.W. Hansen, S.S. Keller, Stereolithography-derived three-dimensional pyrolytic carbon/Mn3O4 nanostructures for free-standing hybrid supercapacitor electrodes, ACS Appl. Nano Mater. 5 (2022) 1808–1819, https://doi.org/10.1021/acsanm.1c03251.
[71] G.L. Goh, N. Saengchairat, S. Agarwala, W.Y. Yeong, T. Tran, Sessile droplets containing carbon nanotubes: a study of evaporation dynamics and CNT alignment for printed electronics, Nanoscale 11 (2019) 10,603–10,614, https://doi.org/10.1039/c9nr03261d.
[72] J. Li, F. Ye, S. Vaziri, M. Muhammed, M.C. Lemme, M. Östling, Efficient inkjet printing of graphene, Adv. Mater. 25 (29) (2013) 3985–3992, https://doi.org/10.1002/adma.201300361.
[73] N.T. Dinh, E. Sowade, T. Blaudeck, S. Hermann, R.D. Rodriguez, D.R. Zahn, S.E. Schulz, R.R. Baumann, O. Kanoun, High-resolution inkjet printing of conductive carbon nanotube twin lines utilizing evaporation-driven self-assembly, Carbon 96 (2016) 382–393, https://doi.org/10.1016/j.carbon.2015.09.072.
[74] S.T. Beyer, K. Walus, Controlled orientation and alignment in films of single-walled carbon nanotubes using inkjet printing, Langmuir 28 (2012) 8753–8759, https://doi.org/10.1021/la300770b.
[75] A. Sola, Materials requirements in fused filament fabrication: a framework for the design of next-generation 3D printable thermoplastics and composites, Macromol. Mater. Eng. 307 (10) (2022), https://doi.org/10.1002/mame.202200197 eid:2200197.
[76] A. Sola, A. Trinchi, 11 - open challenges and future opportunities in fused deposition modeling of composite materials, in: A. Sola, A. Trinchi (Eds.), Fused Deposition Modeling of Composite Materials, 1st ed., U.K.: Elsevier - Woodhead Publishing Series in Composites Science and Engineering, Cambridge, MA, U.S.A. – Kidlington, 2022, pp. 289–328, https://doi.org/10.1016/B978-0-323-98823-0.00002-0.
[77] A. Dorigato, V. Moretti, S. Dul, S. Unterberger, A. Pegoretti, Electrically conductive nanocomposites for fused deposition modelling, Synth. Met. 226 (2017) 7–14, https://doi.org/10.1016/j.synthmet.2017.01.009.
[78] S. Gantenbein, K. Masania, W. Woigk, J.P.W. Sesseg, T.A. Tervoort, A.R. Studart, Three-dimensional printing of hierarchical liquid-crystal-polymer structures, Nature 561 (2018) 226–230, https://doi.org/10.1038/s41586-018-0474-7.
[79] F. Yang, R. Pitchumani, Healing of thermoplastic polymers at an interface under nonisothermal conditions, Macromolecules 35 (2002) 3213–3224, https://doi.org/10.1021/ma010858o.
[80] C. McIlroy, P.D. Olmsted, Deformation of an amorphous polymer during the fused-filament-fabrication method for additive manufacturing, J. Rheol. 61 (2017) 379–397, https://doi.org/10.1122/1.4976839.
[81] A.K. Rajasekharan, R. Bordes, C. Sandström, M. Ekh, M. Andersson, Hierarchical and heterogeneous bioinspired composites—merging molecular self-assembly with additive manufacturing, Small 13 (2017), https://doi.org/10.1002/smll.201700550 eid:1700550.
[82] A. Le Duigou, D. Correa, M. Ueda, R. Matsuzaki, M. Castro, A review of 3D and 4D printing of natural fibre biocomposites, Mater. Des. 194 (2020), https://doi.org/10.1016/j.matdes.2020.108911 eid:108911.
[83] D.E. Yunus, W. Shi, S. Sohrabi, Y. Liu, Shear induced alignment of short nanofibers in 3D printed polymer composites, Nanotechnology 27 (2016), https://doi.org/10.1088/0957-4484/27/49/495302 eid:495302.
[84] G. Trujillo-de Santiago, M.M. Alvarez, M. Samandari, G. Prakash, G. Chandrabhatla, P.I. Rellstab-Sánchez, B. Byambaa, P.P.S.S. Abadi, S. Mandla, R.K. Avery, A. Vallejo-Arroyo, A. Nasajpour, N. Aanabi, Y.S. Zhang, A. Khademhosseini, Chaotic printing: using chaos to fabricate densely packed micro-and nanostructures at high resolution and speed, Mater. Horiz. 5 (2018) 813–822, https://doi.org/10.1039/c8mh00344k.
[85] J. Arrieta, J.H.E. Cartwright, E. Gouillart, N. Piro, O. Piro, I. Tuval, Geometric mixing, Phil. Transac. Royal Soc. A 378 (2020), https://doi.org/10.1098/rsta.2020.0168 eid:20200168.
[86] G. Wang, H. Ouyang, C. Fan, Q. Guo, Z. Li, W. Yan, Z. Li, The origin of high-density dislocations in additively manufactured metals, Mater. Res. Lett. 8 (2020) 283–290, https://doi.org/10.1080/21663831.2020.1751739.
[87] B. Ramaswami, Defect structures produced by cyclic deformation, Bull. Mater. Sci. 12 (1989) 195–206, https://doi.org/10.1007/BF02747131.
[88] Z. Li, Y. Cui, W. Yan, D. Zhang, Y. Fang, Y. Chen, Q. Yu, G. Wang, H. Ouyang, C. Fan, et al., Enhanced strengthening and hardening via self-stabilized dislocation network in additively manufactured metals, Mater. Today 50 (2021) 79–88, https://doi.org/10.1016/j.mattod.2021.06.002.
[89] A. Griffin, Y. Guo, Z. Hu, J. Zhang, Y. Chen, Z. Qiang, Scalable methods for directional assembly of fillers in polymer composites: creating pathways for improving material properties, Polym. Compos. 2022 (2022) 1–20, https://doi.org/10.1002/pc.26905.
[90] T. Coombs, 4 - bulk high temperature superconductor (HTS) materials, in: High Temperature Superconductors (HTS) for Energy Applications, Ser. Woodhead Publishing Series in Energy, Z. Melhem, Woodhead Publishing, Cambridge, U.K. -

Philadelphia, PA, U.S.A. - New Delhi, India, 2012, pp. 101–139, https://doi.org/10.1533/9780857095299.1.101.
[91] R.K. Kotnala, J. Shah, in: K. Buschow (Ed.), 4 - Ferrite Materials: Nano to Spintronics Regime," Ser. Handbook of Magnetic Materials, The Netherland - Oxford, U.K, 23, North-Holland, Elsevier, 2015, pp. 291–379, https://doi.org/10.1016/B978-0-444-63528-0.00004-8.
[92] E. Spain, A. Venkatanarayanan, 13.02 - review of physical principles of sensing and types of sensing materials, in: S. Hashmi, G.F. Batalha, C.J. Van Tyne, B. Yilbas (Eds.), Comprehensive Materials Processing, Elsevier, Oxford, U.K., 2014, pp. 5–46, https://doi.org/10.1016/B978-0-08-096532-1.01302-9.
[93] D. Givord, H. Li, J. Moreau, Magnetic properties and crystal structure of nd2fe14b, Solid State Commun. 50 (1984) 497–499, https://doi.org/10.1016/0038-1098(84)90315-6.
[94] W.J. Chong, S. Shen, Y. Li, A. Trinchi, D. Pejak, I.L. Kyratzis, A. Sola, C. Wen, Additive manufacturing of antibacterial PLA-ZnO nanocomposites: benefits, limitations and open challenges, J. Mater. Sci. Technol. 111 (2022) 120–151, https://doi.org/10.1016/j.jmst.2021.09.039.
[95] V. Marghussian, 4 - magnetic properties of nano-glass ceramics, in: V. Marghussian (Ed.), Nano-Glass Ceramics, William Andrew Publishing, Oxford, U.K., 2015, pp. 181–223, https://doi.org/10.1016/B978-0-323-35386-1.00004-9.
[96] D. Kokkinis, M. Schaffner, A.R. Studart, Multimaterial magnetically assisted 3D printing of composite materials, Nat. Commun. 6 (2015), https://doi.org/10.1038/ncomms9643 eid:8643.
[97] R.M. Erb, R. Libanori, N. Rothfuchs, A.R. Studart, Composites reinforced in three dimensions by using low magnetic fields, Science 335 (6065) (2012) 199–204, https://doi.org/10.1126/science.1210822.
[98] J.J. Martin, B.E. Fiore, R.M. Erb, Designing bioinspired composite reinforcement architectures via 3D magnetic printing, Nat. Commun. 6 (2015), https://doi.org/10.1038/ncomms9641 eid:8641.
[99] T. Nakamoto, S. Marukado, Properties of photopolymer part with aligned short ferromagnetic fibers, Int. J. Autom. Technol. 10 (6) (2016) 916–922, https://doi.org/10.20965/ijat.2016.p0916.
[100] Y. Kim, H. Yuk, R. Zhao, S.A. Chester, X. Zhao, Printing ferromagnetic domains for untethered fast-transforming soft materials, Nature 558 (2018) 274–279, https://doi.org/10.1038/s41586-018-0185-0.
[101] J.Z. Manapat, Q. Chen, P. Ye, R.C. Advincula, 3D printing of polymer nanocomposites via stereolithography, Macromol. Mater. Eng. 302 (9) (2017), https://doi.org/10.1002/mame.201600553 eid:1600553.
[102] P.D. Dalton, C. Vaquette, B.L. Farrugia, T.R. Dargaville, T.D. Brown, D.W. Hutmacher, Electrospinning and additive manufacturing: converging technologies, Biomater. Sci. 1 (2) (2013) 171–185, https://doi.org/10.1039/C2BM00039C.
[103] J.A. Smith, E. Mele, Electrospinning and additive manufacturing: adding three-dimensionality to electrospun scaffolds for tissue engineering, Front. Bioeng. Biotechnol. 9 (2021), https://doi.org/10.3389/fbioe.2021.674738 eid:674738.
[104] H. Abdolmaleki, P. Kidmose, S. Agarwala, Droplet-based techniques for printing of functional inks for flexible physical sensors, Adv. Mater. 33 (20) (2021), https://doi.org/10.1002/adma.202006792 eid:2006792.
[105] S. Cai, Y. Sun, Z. Wang, W. Yang, X. Li, H. Yu, Mechanisms, influencing factors, and applications of electrohydrodynamic jet printing, Nanotechnol. Rev. 10 (2021) 1046–1078, https://doi.org/10.1515/ntrev-2021-0073.
[106] A.S.K. Kiran, J.B. Veluru, S. Merum, A. Radhamani, M. Doble, T.S. Kumar, S. Ramakrishna, Additive manufacturing technologies: an overview of challenges and perspective of using electrospraying, Nanocomposites 4 (2018) 190–214, https://doi.org/10.1080/20550324.2018.1558499.
[107] M.M. Nazemi, A. Khodabandeh, A. Hadjizadeh, Near-field electrospinning: crucial parameters, challenges, and applications, ACS Appl. Bio Mater. 5 (2022) 394–412, https://doi.org/10.1021/acsabm.1c00944.
[108] L.R. Holmes, J.C. Riddick, Research summary of an additive manufacturing technology for the fabrication of 3D composites with tailored internal structure, JOM (J. Occup. Med.) 66 (2) (2014) 270–274, https://doi.org/10.1007/s11837-013-0828-4.
[109] D. Pejak Simunec, A. Sola, Emerging research in conductive materials for fused filament fabrication: a critical review, Adv. Eng. Mater. 24 (2022), https://doi.org/10.1002/adem.202101476 eid:2101476.
[110] D.A. Porter, T.V.T. Hoang, T.A. Berfield, Effects of in-situ poling and process parameters on fused filament fabrication printed PVDF sheet mechanical and electrical properties, Addit. Manuf. 13 (2017) 81–92, https://doi.org/10.1016/j.addma.2016.11.005.
[111] L. Koroglu, E. Ayas, N. Ay, 3D printing of polyvinylidene fluoride based piezoelectric nanocomposites: an overview, Macromol. Mater. Eng. 306 (10) (2021), https://doi.org/10.1002/mame.202100277 eid:2100277.
[112] Y. Hu, Recent progress in field-assisted additive manufacturing: materials, methodologies, and applications, Mater. Horiz. 8 (3) (2021) 885–911, https://doi.org/10.1039/d0mh01322f.
[113] Y. Sriphutkiat, S. Kasetsirikul, D. Ketpun, Y. Zhou, Cell alignment and accumulation using acoustic nozzle for bioprinting, Sci. Rep. 9 (2019), https://doi.org/10.1038/s41598-019-54330-8 eid:17774.
[114] A. Lenshof, T. Laurell, Acoustic contrast factor, in: B. Bhushan (Ed.), Encyclopedia of Nanotechnology, Springer Netherlands, Dordrecht, 2012, pp. 30–31, https://doi.org/10.1007/978-90-481-9751-4 425.
[115] L. Meng, F. Cai, F. Li, W. Zhou, L. Niu, H. Zheng, Acoustic tweezers, J. Phys. Appl. Phys. 52 (2019), https://doi.org/10.1088/1361-6463/ab16b5 eid:273001.
[116] H.O. Fatoyinbo, Microfluidic devices for cell manipulation, in: X.J. Li, Y. Zhou (Eds.), Microfluidic Devices for Biomedical Applications, Elsevier, Philadelphia, PA, U.S.A. - New Delhi, India, 2021, pp. 329–389, https://doi.org/10.1533/9780857097040.3.283.
[117] Chapter 6 - physics of electrorheological fluids, in: T. Hao (Ed.), Electrorheological Fluids, Ser. Studies in Interface Science, 22, U.K. - London, U.K.: Elsevier, Amsterdam, The Netherlands - San Diego, CA, U.S.A. - Kidlington, 2005, pp. 235–340, https://doi.org/10.1016/S1383-7303(05)80021-3.
[118] S. Yamahira, S.-i. Hatanaka, M. Kuwabara, S. Asai, Orientation of fibers in liquid by ultrasonic standing waves, Jpn. J. Appl. Phys. 39 (6A) (2000) 3683–3687, https://doi.org/10.1143/JJAP.39.3683.
[119] T.M. Llewellyn-Jones, B.W. Drinkwater, R.S. Trask, 3D printed components with ultrasonically arranged microscale structure, Smart Mater. Struct. 25 (2016), https://doi.org/10.1088/0964-1726/25/2/02LT01 eid:02LT01.
[120] I. Bernard, A.A. Doinikov, P. Marmottant, D. Rabaud, C. Poulain, P. Thibault, Controlled rotation and translation of spherical particles or living cells by surface acoustic waves, Lab Chip 17 (14) (2017) 2470–2480, https://doi.org/10.1039/C7LC00084G.
[121] K. Johnson, D. Melchert, D.S. Gianola, M. Begley, T.R. Ray, Recent progress in acoustic field-assisted 3D-printing of functional composite materials, MRS Advan. 6 (2021) 636–643, https://doi.org/10.1557/s43580-021-00090-5.
[122] X. Li, K.M. Lim, W. Zhai, A novel class of bioinspired composite via ultrasound-assisted directed self-assembly digital light 3D printing, Appl. Mater. Today 26 (2022), https://doi.org/10.1016/j.apmt.2022.101388 eid:101388.
[123] F. Demoly, J.C. André, Is order creation through disorder in additive manufacturing possible? Cogent Eng. 8 (2021) https://doi.org/10.1080/23311916.2021.1889110 eid:1889110.
[124] Y. Yang, G. Wang, H. Liang, C. Gao, S. Peng, L. Shen, C. Shuai, Additive manufacturing of bone scaffolds, Inter. J. Bioprinting 5 (2019), https://doi.org/10.18063/IJB.v5i1.148 eid:148.
[125] J.S. Cuellar, G. Smit, D. Plettenburg, A. Zadpoor, Additive manufacturing of non-assembly mechanisms, Addit. Manuf. 21 (2018) 150–158, https://doi.org/10.1016/j.addma.2018.02.004.
[126] A.I. Mertens, Chapter 13 - metal matrix composites processed by laser additive manufacturing: microstructure and properties, in: J. Pou, A. Riveiro, J.P. Davim (Eds.), Additive Manufacturing, Ser. Handbooks in Advanced Manufacturing, U.K. - Cambridge, MA, U.S.A.: Elsevier, Amsterdam, The Netherlands - Kidlington, 2021, pp. 409–425, https://doi.org/10.1016/B978-0-12-818411-0.00005-7.
[127] D. Du, A. Dong, D. Shu, D. Wang, G. Zhu, B. Sun, E.J. Lavernia, Influence of static magnetic field on the microstructure of nickel-based superalloy by laser-directed energy deposition, Metall. Mater. Trans. 51 (2020) 3354–3359, https://doi.org/10.1007/s11661-020-05783-4.
[128] N. Kang, H. Yuan, P. Coddet, Z. Ren, C. Bernage, H. Liao, C. Coddet, On the texture, phase and tensile properties of commercially pure Ti produced via selective laser melting assisted by static magnetic field, Mater. Sci. Eng. C 70 (2017) 405–407, https://doi.org/10.1016/j.msec.2016.09.011.
[129] C. Todaro, M. Easton, D. Qiu, D. Zhang, M. Bermingham, E. Lui, M. Brandt, D. StJohn, M. Qian, Grain structure control during metal 3D printing by high-intensity ultrasound, Nat. Commun. 11 (2020), https://doi.org/10.1038/s41467-019-13874-z eid:142.
[130] H. Zhou, C. Song, Y. Yang, C. Han, M. Wang, Y. Xiao, Z. Liu, The microstructure and properties evolution of SS316L fabricated by magnetic field-assisted laser powder bed fusion, Mater. Sci. Eng., A 845 (2022), https://doi.org/10.1016/j.msea.2022.143216 eid:143216.
[131] W.H. Yu, S.L. Sing, C.K. Chua, C.-N. Kuo, X.L. Tian, Particle-reinforced metal matrix nanocomposites fabricated by selective laser melting: a state of the art review, Prog. Mater. Sci. 104 (2019) 330–379, https://doi.org/10.1016/j.pmatsci.2019.04.006.
[132] M. Qu, Q. Guo, L.I. Escano, S.J. Clark, K. Fezzaa, L. Chen, Mitigating keyhole pore formation by nanoparticles during laser powder bed fusion additive manufacturing, Additive Manufac. Lett. 3 (2022), https://doi.org/10.1016/j.addlet.2022.100068 eid:100068.
[133] F. Yang, L. Wang, Z. Wang, Q. Wu, K. Zhou, X. Lin, W. Huang, Ultra strong and ductile eutectic high entropy alloy fabricated by selective laser melting, J. Mater. Sci. Technol. 106 (2022) 128–132, https://doi.org/10.1016/j.jmst.2021.08.015.
[134] X. Gao, S. Qi, X. Kuang, Y. Su, J. Li, D. Wang, Fused filament fabrication of polymer materials: a review of interlayer bond, Addit. Manuf. 37 (2021), https://doi.org/10.1016/j.addma.2020.101658 eid:101658.
[135] T.J. Gordelier, P.R. Thies, L. Turner, L. Johanning, Optimising the FDM additive manufacturing process to achieve maximum tensile strength: a state-of-the-art review, Rapid Prototyp. J. 25 (2019) 953–971, https://doi.org/10.1108/RPJ-07-2018-0183.
[136] M. Padole, S. Gharde, B. Kandasubramanian, Three-dimensional printing of molluscan shell inspired architectures via fused deposition modeling, Environ. Sci. Pollut. Control Ser. 28 (2021) 46,356–46,366, https://doi.org/10.1007/s11356-020-09799-6.
[137] P.K. Penumakala, J. Santo, A. Thomas, A critical review on the fused deposition modeling of thermoplastic polymer composites, Compos. B Eng. 201 (2020), https://doi.org/10.1016/j.compositesb.2020.108336 eid:108336.
[138] S.D. Cakal, C. Radeke, J.F. Alcala, D.G. Ellman, S. Butdayev, D.C. Andersen, K. Calloe, J.U. Lind, A simple and scalable 3D printing methodology for generating aligned and extended human and murine skeletal muscle tissues, Biomed. Mater. 17 (2022), https://doi.org/10.1088/1748-605X/ac6b71 eid:045013.
[139] M.A.S.R. Saadi, A. Maguire, N.T. Pottackal, M.S.H. Thakur, M.M. Ikram, A.J. Hart, P.M. Ajayan, M.M. Rahman, Direct ink writing: a 3D printing technology for diverse materials, Adv. Mater. 34 (2022), https://doi.org/10.1002/adma.202108855 eid:2108855.

[140] Y. Cheng, K.H. Chan, X.-Q. Wang, T. Ding, T. Li, X. Lu, G.W. Ho, Direct-ink-write 3D printing of hydrogels into biomimetic soft robots, ACS Nano 13 (2019) 13,176–13,184, https://doi.org/10.1021/acsnano.9b06144.
[141] R.C. Advincula, J.R.C. Dizon, E.B. Caldona, R.A. Viers, F.D.C. Siacor, R.D. Maalihan, A.H. Espera, On the progress of 3D-printed hydrogels for tissue engineering, MRS Commun. 11 (5) (2021) 539–553, https://doi.org/10.1557/s43579-021-00069-1.
[142] Ż. Górecka, J. Idaszek, D. Kołbuk, E. Choińska, A. Chlanda, W. Świkeszkowski, The effect of diameter of fibre on formation of hydrogen bonds and mechanical properties of 3D-printed PCL, Mater. Sci. Eng. C 114 (2020), https://doi.org/10.1016/j.msec.2020.111072 eid:111072.
[143] S. Safaee, M. Schock, E.B. Joyee, Y. Pan, R.K. Chen, Field-assisted additive manufacturing of polymeric composites, Addit. Manuf. 51 (2022), 102642, https://doi.org/10.1016/j.addma.2022.102642.
[144] Y. Yang, Z. Chen, X. Song, Z. Zhang, J. Zhang, K.K. Shung, Q. Zhou, Y. Chen, Biomimetic anisotropic reinforcement architectures by electrically assisted nanocomposite 3D printing, Adv. Mater. 29 (2017), https://doi.org/10.1002/adma.201605750 eid:1605750.
[145] Y. Bouligand, Twisted fibrous arrangements in biological materials and cholesteric mesophases, Tissue Cell 4 (1972) 189–217, https://doi.org/10.1016/S0040-8166(72)80042-9.
[146] B. Natarajan, J.W. Gilman, Bioinspired Bouligand cellulose nanocrystal composites: a review of mechanical properties, Phil. Trans. Math. Phys. Eng. Sci. 376 (2112) (2018), https://doi.org/10.1098/rsta.2017.0050 eid:20170050.
[147] Q. Zhang, F. Zhang, S.P. Medarametla, H. Li, C. Zhou, D. Lin, 3D printing of graphene aerogels, Small 12 (2016) 1702–1708, https://doi.org/10.1002/smll.201503524.
[148] M. Helms, S.S. Vattam, A.K. Goel, Biologically inspired design: process and products, Des. Stud. 30 (5) (2009) 606–622, https://doi.org/10.1016/j.destud.2009.04.003.
[149] P. Fratzl, R. Weinkamer, Nature's hierarchical materials, Prog. Mater. Sci. 52 (2007) 1263–1334, https://doi.org/10.1016/j.pmatsci.2007.06.001.
[150] The state of 3D printing – 2021 Edition, Sculpteo, 10 Rue Auguste Perret, 94800 Villejuif, France, Survey [Online]. Available: https://www.sculpteo.com/en/ebooks/state-of-3d-printing-report-2021/, 2021.
[151] H. Canziani, S. Chiera, T. Schuffenhauer, S.-P. Kopp, F. Metzger, A. Bück, M. Schmidt, N. Vogel, Bottom-up design of composite supraparticles for powder-based additive manufacturing, Small 16 (2020), https://doi.org/10.1002/smll.202002076 eid:2002076.
[152] H. Canziani, F. Bever, A. Sommereyns, M. Schmidt, N. Vogel, Roughly spherical: tailored PMMA–SiO2 composite supraparticles with optimized powder flowability for additive manufacturing, ACS Appl. Mater. Interfaces 13 (2021) 25,334–25,345, https://doi.org/10.1021/acsami.1c02264.
[153] H. Canziani, B. Hanschmann, F. Tischer, A. Sommereyns, T. Distler, J. Schramm, N. Hesse, J. Schmidt, A. Grünewald, R. Detsch, et al., Biodegradable polylactide supraparticle powders with functional additives for biomedical additive manufacturing, Adv. Funct. Mater. (2022), https://doi.org/10.1002/adfm.202205730 eid:2205730.
[154] S.C. Glotzer, M.J. Solomon, Anisotropy of building blocks and their assembly into complex structures, Nat. Mater. 6 (2007) 557–562, https://doi.org/10.1038/nmat1949.
[155] H. Long, L. Hu, F. Yang, Q. Cai, Z. Zhong, S. Zhang, L. Guan, D. Xiao, W. Zheng, W. Zhou, Y. Wei, K. Frank, X. Dong, Enhancing the performance of polylactic acid composites through self-assembly lignin nanospheres for fused deposition modeling, Compos. B Eng. 239 (2022), https://doi.org/10.1016/j.compositesb.2022.109968 eid:109968.
[156] A. Hernández-Sosa, R.A. Ramírez-Jiménez, L. Rojo, F. Boulmedais, M.R. Aguilar, M. Criado-Gonzalez, R. Hernández, Optimization of the rheological properties of self-assembled tripeptide/alginate/cellulose hydrogels for 3D printing, Polymers 14 (2022), https://doi.org/10.3390/polym14112229 eid:2229.
[157] J. Park, N. Jeon, S. Lee, G. Choe, E. Lee, J.Y. Lee, Conductive hydrogel constructs with three-dimensionally connected graphene networks for biomedical applications, Chem. Eng. J. 446 (2022), https://doi.org/10.1016/j.cej.2022.137344 eid:137344.
[158] J. Yin, J. Zhong, J. Wang, Y. Wang, T. Li, L. Wang, Y. Yang, Z. Zhen, Y. Li, H. Zhang, S. Zhong, Y. Wu, W. Huang, 3D-printed high-density polyethylene scaffolds with bioactive and antibacterial layer-by-layer modification for auricle reconstruction, Mater. Today Bio. 16 (2022), https://doi.org/10.1016/j.mtbio.2022.100361 eid:100361.
[159] J. Zhou, X. Wu, Y. Chen, C. Yang, R. Yang, J. Tan, Y. Liu, L. Qiu, H.-M. Cheng, 3D printed template-directed assembly of multiscale graphene structures, Adv. Funct. Mater. 32 (2022), https://doi.org/10.1002/adfm.202105879 eid:2105879.
[160] C. Yang, X. Wu, H. Xia, J. Zhou, Y. Wu, R. Yang, G. Zhou, L. Qiu, 3D printed template-assisted assembly of additive-free Ti3C2Tx MXene microlattices with customized structures toward high areal capacitance, ACS Nano 16 (2022) 2699–2710, https://doi.org/10.1021/acsnano.1c09622.
[161] Q. Zhang, F. Zhang, X. Xu, C. Zhou, D. Lin, Three-dimensional printing hollow polymer template-mediated graphene lattices with tailorable architectures and multifunctional properties, ACS Nano 12 (2018) 1096–1106, https://doi.org/10.1021/acsnano.7b06095.
[162] Y. Song, S. Hua, S. Sayyar, Z. Chen, J. Chung, X. Liu, Z. Yue, C. Angus, B. Filippi, S. Beirne, W. Gordon, G. Sutton, J. You, Corneal bioprinting using a high concentration pure collagen I transparent bioink, Bioprinting 28 (2022), https://doi.org/10.1016/j.bprint.2022.e00235 eid:e00235.
[163] E. Sanchez-Rexach, T.G. Johnston, C. Jehanno, H. Sardon, A. Nelson, Sustainable materials and chemical processes for additive manufacturing, Chem. Mater. 32 (2020) 7105–7119, https://doi.org/10.1021/acs.chemmater.0c02008.
[164] D.V. Baker, C. Bao, W.S. Kim, Highly conductive 3D printable materials for 3D structural electronics, Appl. Electron. Mater. 3 (2021) 2423–2433, https://doi.org/10.1021/acsaelm.1c00296.
[165] J.-Y. Lee, W.S. Tan, J. An, C.K. Chua, C.Y. Tang, A.G. Fane, T.H. Chong, The potential to enhance membrane module design with 3D printing technology, J. Membr. Sci. 499 (2016) 480–490, https://doi.org/10.1016/j.memsci.2015.11.008.
[166] A. Soo, S.M. Ali, H.K. Shon, 3D printing for membrane desalination: challenges and future prospects, Desalination 520 (2021), https://doi.org/10.1016/j.desal.2021.115366 eid:115366.
[167] L.D. Tijing, J.R.C. Dizon, I. Ibrahim, A.R.N. Nisay, H.K. Shon, R.C. Advincula, 3D printing for membrane separation, desalination and water treatment, Appl. Mater. Today 18 (2020), https://doi.org/10.1016/j.apmt.2019.100486 eid:100486.
[168] Z. Chen, Z. Li, J. Li, C. Liu, C. Lao, Y. Fu, C. Liu, Y. Li, P. Wang, Y. He, 3D printing of ceramics: a review, J. Eur. Ceram. Soc. 39 (2019) 661–687, https://doi.org/10.1016/j.jeurceramsoc.2018.11.013.